



HAL
open science

Thermodynamic modeling of Cr and Cr–H systems up to high temperatures and high pressures

Maxime Dottor, Jean-Claude Crivello, Jean-Marc Joubert

► **To cite this version:**

Maxime Dottor, Jean-Claude Crivello, Jean-Marc Joubert. Thermodynamic modeling of Cr and Cr–H systems up to high temperatures and high pressures. *International Journal of Hydrogen Energy*, 2022, 47 (55), pp.23293-23309. 10.1016/j.ijhydene.2022.04.245 . hal-03747843

HAL Id: hal-03747843

<https://hal.science/hal-03747843>

Submitted on 8 Aug 2022

HAL is a multi-disciplinary open access archive for the deposit and dissemination of scientific research documents, whether they are published or not. The documents may come from teaching and research institutions in France or abroad, or from public or private research centers.

L'archive ouverte pluridisciplinaire **HAL**, est destinée au dépôt et à la diffusion de documents scientifiques de niveau recherche, publiés ou non, émanant des établissements d'enseignement et de recherche français ou étrangers, des laboratoires publics ou privés.

Thermodynamic modeling of Cr and Cr–H systems up to high temperatures and high pressures

Maxime Dottor^a, Jean-Claude Crivello^a, Jean-Marc Joubert^{a,*}

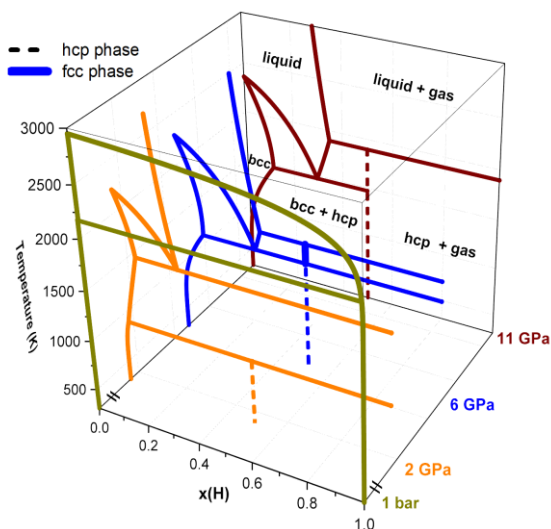
^a Univ Paris Est Creteil, CNRS, ICMPE, UMR 7182, 2 rue Henri Dunant, 94320 Thiais, France

* Corresponding author. jean-marc.joubert@cnr.fr

ABSTRACT:

A complete literature review of the thermodynamic and phase diagram properties of pure Cr and Cr–H system has been carried out. A thermodynamic assessment using the Calphad method has been accomplished up to 50 GPa for Cr including the liquid phase and up to 18 GPa on the Cr–H system using the most relevant literature data and our own ab-initio calculations. An up-to-date phase diagram of the Cr–H system is presented. Special attention was paid to the *fcc* phase to clarify the structure type (NaCl, hydrogen atoms located in the octahedral site of the *fcc* structure) and the composition (one hydrogen per chromium atom). The robustness of our proposed Cr and Cr–H models was demonstrated by comparing our measurements of pressure-composition isotherms of a *bcc* Cr–Zr alloy with the prediction made by combining the thermodynamic descriptions of the three Cr–H, H–Zr and Cr–Zr binary systems.

GRAPHICAL ABSTRACT:



KEYWORDS: Cr–H, Cr–H–Zr, metal hydride, Calphad, bcc, high-pressure.

HIGHLIGHTS:

- A complete review of the Cr and the Cr–H systems is displayed. The 3-dimension phase diagram of Cr–H is shown.
- Thermodynamic modeling of the chromium Cr and Cr–H systems is displayed for the first time.
- Unary and binary models are checked by comparing extrapolation of Cr–H–Zr system and hydrogen properties of Cr₅Zr₉₅ alloy.

1. INTRODUCTION

Hydrides formed by transition metal alloys or intermetallic compounds are attractive hydrogen storage materials. In transition metal based hydrogen storage materials [1], hydrogen is located in the interstitial sites such as the octahedral or the tetrahedral sites. Body centered cubic (*bcc*) solid solutions based on Ti and V are one example of interesting materials. They have been used in the past decades because of a high hydrogen capacity, i.e. more than two weight percent at room temperature [2–5], and their interest has been renewed recently through the use of complex compositions known as high entropy alloys [6,7]. These *bcc* alloys are often made up by alloying light transition metals with chromium. Thus, the knowledge of the hydrogen interaction with this metal appears to be essential. However, an up-to-date complete literature review and thermodynamic assessment of Cr–H system are lacking. These are all the more important as Cr is also a major component in stainless steel and in Laves phases hydrogen storage alloys [8]. The Cr–H system contains five phases: *bcc*, two different hydrides of composition CrH, the liquid and gas phases. The hydrides can be synthesized only at high–pressure [9–11].

A Calphad type thermodynamic assessment at high pressure requires a proper description of the volume of the different phases using a relevant equation of state (EOS). For this purpose, an EOS to describe the high pressure and high temperature data has been developed by Lu et al. [12] and modified by Joubert et al. [13]. Nonetheless, this description requires a complete assessment of pure Cr and ab-initio calculations for the hydrides.

In the present work, a complete literature evaluation is performed. Additionally, description of Cr and Cr–H phase diagrams have been performed using the CALPHAD method including the high-pressure model developed by Lu et al. [12] as modified by Joubert et al. [13]. Experimental, first principles and quasi-harmonic phonon calculated data have been considered to assess these systems. The assessment of Cr and the Cr–H systems was performed up to 50 GPa and 18 GPa, respectively. The reliability of our unary and binary thermodynamic descriptions was tested by examining our pressure-composition isotherms determined experimentally against the prediction made from the extrapolation of the Cr–H–Zr system. The first part of this paper is dedicated to the literature review of the Cr and Cr–H, the second part is dedicated to the methods and the last part to the results.

2. CR AND CR-H SYSTEMS: STATE OF THE ART

2.1 Experimental data on Cr.

Table 1 – Experimental temperature and pressure dependent volume data on Cr.

Phase	Data type	Range	Technique	Reference	Used	
<i>bcc</i>	<i>V-T</i> at $p=10^5$ Pa	283-333 K	XRD ^b	[14]	Yes	
		1073-1973 K	XRD ^b	[15]	Yes	
		77-500 K	XRD ^b	[16]	No	
		292-2073 K	XRD ^b	[17]	Yes	
		293-1773 K	XRD ^b	[18]	Yes	
		296 K	XRD ^b	[19]	No	
		89-469 K	XRD ^b	[20]	Comp ^a	
		276-352 K	XRD ^b	[21]	Yes	
		1003-2008 K	Penetrating γ -radiation	[22]	No	
		293-2100 K	Penetrating γ -radiation	[23]	Comp ^a	
		298-2100 K	XRD ^b	[24]	Comp ^a	
		<i>α-T</i> at $p=10^5$ Pa	67-263 K	Interferometry	[25]	Comp ^a
			312-921 K	Interferometry	[26]	Comp ^a
103-473 K	Interferometry		[27]	Comp ^a		
293-2131 K	Penetrating γ -radiation		[23]	No		
500-1880 K	Push-rod dilatometry		[28]	Yes		
298-2149 K	SXRD ^c		[24]	Yes		
	<i>V-p</i> at 298 K	0-8.3 GPa (293 K)	hp XRD ^d	[29]	Yes	

		0-36.8 GPa	hp XRD ^d	[30]	No
		0-84 GPa	hp XRD ^d	[31]	Yes
		4.67-40.4 GPa	hp SRXD ^c	[11]	Yes
	<i>B-T</i>	77-500 K	Ultrasonic resonance	[16]	No
		1-330 K	Ultrasonic pulse-echo	[32]	Comp ^a
		125-707 K	Sound velocity	[33]	Yes
		320-550 K	Ultrasonic pulse-echo	[34]	Comp ^a
		350-1600 K	Sound velocity	[35]	Yes
	Hugoniot	0-129 GPa	Shock wave	[36]	Yes
<i>liquid</i>	<i>V-T</i>	2166-2500 K	Imaging, levitation	[37]	Yes
		2101-2242 K	Penetrating γ -radiation	[22]	No
		2140-2342 K	Penetrating γ -radiation	[23]	Partly yes
	<i>T_m-P</i>	7.48-63.21 GPa	Optical, DAC ^e	[38]	Yes

^a Comp: only for comparison

^b XRD: X-Ray Diffraction

^c SXR: Synchrotron X-Ray Diffraction

^d hp XRD: High pressure X-Ray Diffraction

^e DAC: Diamond-Anvil-Cell

The high-pressure and high-temperature data for pure *bcc* chromium are numerous [11,14–36] (**Table 1**). The molar volume $V_m^{Cr,bcc}$ variations with temperature and/or pressure were determined using diffraction, penetrating γ -radiation and shock-wave experiment. The *bcc* chromium thermal expansivity $\alpha^{Cr,bcc}$ was studied by interferometry [25–27], penetrating

γ -radiation [23], dilatometry [28] and diffraction [24] and the bulk modulus temperature dependence $B^{Cr,bcc}$ was collected up to 1600 K [16,32–35].

In the assessment, some experimental data were excluded [16,19,22,23,30]. It is believed that this data has been altered by contamination either during the sample preparation or during their measurements [16,19,22,23] and measurements from Tkacz et al. [30] were rejected due to the absence of a quasihydrostatic pressure medium in their experiment according to Marizy et al. [11].

The melting curve was measured by Errandonea et al. [38]. The temperature dependence of the liquid chromium molar volume was collected up to 2500 K [22,23,37]. In this assessment, the data from Saito et al. [37] was used, the data of Stankus [23] was partly used and the data of Makeev and Popev [22] was rejected. It is believed that a contamination was occurring during their experiments (mainly by oxygen) or that technical issues were encountered during the measurement due to the very high vapor pressure of chromium [39]. As a result, the molar volumes found are too high.

2.2 Experimental data on hydrides in the Cr–H system.

The hydride CrH₃ was described long time ago in the literature [40,41], since then, this phase was not mentioned, so its existence is very uncertain, and it was excluded from this assessment. Recently, super hydrides have been synthesized [11] ; Cr₂H₃ (*C2/m* space group) was found when the pressure has been increased above 19 GPa, and CrH₂ (*Pnma*) appeared above 31 GPa. These super hydrides were not considered in the present assessment. Therefore, the maximum pressure allowed in this work is limited at 18 GPa.

Table 2 – Experimental temperature and pressure dependent volume data on the Cr–H system.

Phase	Data type	Range	Technique	Reference	Used
<i>hcp</i>	<i>V-T</i> at $p=10^5$ Pa	284-298 K	XRD	[42]	Yes
		298 K	XRD	[43]	Yes

		298 K	XRD	[44]	Yes
		423 K	XRD	[45]	Yes
		298 K	XRD	[30]	Yes
		276 K	XRD	[46]	Yes
		8 K	SXRD	[47]	Comp ^a
		298 K	SXRD	[11]	Yes
	<i>V-p</i> at 298 K	0-36.5 GPa	hp XRD	[30,48]	Comp ^a
		53.1 MPa - 41.1 GPa	hp SXRD	[11]	Yes
	<i>V-T-p</i>	508-1298 K 2-5 GPa	hp SXRD	[10]	Comp ^a
	<i>B-T</i>	298 K	Obtained from Birch- Murnaghan equation	[30]	No
		298 K	Obtained from Vinet equation	[11]	Yes
<i>fcc</i>	<i>V-T</i> at $p=10^5$ Pa	298 K	XRD	[49]	No
		298 K	XRD	[50]	No
		298 K	XRD	[43]	Comp ^a
		298 K	XRD	[44]	Yes.
		298 K	XRD	[30]	Yes
		276 K	XRD	[46]	Yes
		8 K	SXRD	[47]	Yes

$V-p$ at 298 K	0-37 GPa	hp XRD	[30]	Yes
$V-T-p$	1009-1342 K 2-5 GPa	hp SXRD	[10]	Yes
$B-T$	298 K	Obtained from Birch-Murnaghan equation	[30]	No

^a Comp: only for comparison

Some data [10,11,30,42–48] is available for the modeling of hexagonal close-packed *hcp*–CrH at high–pressure and high–temperature and even fewer data [10,30,42–44,46,47,49,50] for the face-centered cubic *fcc*–CrH phase (**Table 2**). Both hydrides are unstable at ambient pressure and are produced either electrolytically [30,42–44,46,47,49,50] or under high hydrogen gas pressure [9–11].

In the assessment of the pure hydride phases, several experimental results were excluded [16,19,22,23,30,49,50] due to possible alteration caused either during the preparation of the samples or during the measurements [16,19,22,23,49,50]. Regarding the bulk modulus of the *hcp*–CrH, two values have been reported by Tkacz [30] and Marizy et al. [11], i.e. 240 GPa and 177 GPa, respectively. The experimental value of Marizy et al. [11] was selected since the decrease of the bulk modulus when the hydrogen content increases is consistent with other metal–hydrogen systems [51].

2.3 Experimental phase diagram and thermodynamic data on the Cr–H system.

Chromium is *bcc* (*A2*, W–type, $Im\bar{3}m$), the structure of the monohydride, CrH (hexagonal, $B8_1$, NiAs–type with chromium located in $\frac{1}{3}, \frac{2}{3}, \frac{1}{4}$ and hydrogen in 0, 0, 0, $P6_3/mmc$) has been long-established by neutron diffraction [52]. The other hydride is cubic ($Fm\bar{3}m$). Discussion about the latter phase is given in the next paragraph.

Table 3 – Experimental data regarding the fcc phase of the Cr–H system.

Synthesis method	H/Cr and technique used	Cell parameter (Å) and technique used	T (K)	Pressure	Ref.
	-	3.85 and XRD	RT	-	
Electrolytically	1.7 and high-temperature gas extraction	-	-	-	[49]
Electrolytically	-	3.8605 and XRD	RT	Atm.	[50]
Electrolytically	1.020 to 1.098 and hot extraction	-	-	-	[42]
Electrolytically	> 1.5 and air-jacketed gas burette	2.878 -(paper) but 3.878 (supposed) and XRD	RT	Atm.	[43]
Electrolytically	< 1.02 and chromatography	3.853 and XRD	RT	Atm.	[44]
Electrolytically to produce <i>fcc</i> and then high-pressure apparatus for experimentation	≈ 1 and mass spectroscopy	3.72 to 3.85 and XRD	RT	Atm to 37 GPa	[30]
High-pressure	-	-	500 to 1400 K	2 to 5.5 GPa	[10]
Electrolytically	1.3(2) and thermal desorption spectroscopy	-	-	-	[46]
	-	3.86 and XRD	RT	Atm.	

Electrolytically	0.93(4) and hot extraction	3.854(3) and PND ^a	8 K	Atm.	[47]
-: No information was found.					
^a PND: Powder Neutron Diffraction.					

The literature data for the cubic phase of the Cr–H system is presented in **Table 3**. From all the X-Ray diffraction patterns, it can be concluded that chromium in this hydride has a *fcc* sublattice, $Fm\bar{3}m$ as space group. Thus, the most probable structure of the hydride is either NaCl (*B1* Strukturbericht) with hydrogen in the octahedral site or CaF₂ with hydrogen in the tetrahedral site (*C1*). Unfortunately, the two structures cannot be distinguished by X-ray diffraction. Another information could be found in the composition since the NaCl structure cannot accommodate more than 1 H atom per metal atom (*H/M*) in the octahedral position (if no metal vacancy is considered) while the CaF₂ structure can accommodate up to 2 *H/M*.

The prototype of this *fcc* phase was first postulated to be CaF₂ [49,50], by analogy with other hydrides of *bcc* metals like vanadium or niobium. Until now, no paper mentioned a successful synthesis of the full dihydride CrH₂. Snavely [49] and Roy and Gibb [43] declared to have made hydrides with H/Cr equal to 1.7 and larger than 1.5, respectively. However, Stock and Hardcastle [44] tried to reproduce the synthesis of Snavely [49] unsuccessfully. At the same time, two publications [42,44] reported the preparation of a *fcc* hydride with a composition H/Cr between 1.02 and 1.10. Miura et al. [46] claimed a H/Cr ratio over 1.0 ; however, no cell parameter dependence as a function of composition is given. Tkacz [30] prepared an atomic H-to-metal ratio of approximately 1 for the *fcc* CrH. Antonov et al. [47] performed neutron diffraction on the *fcc* hydride and CrH_{0.93±0.04} was synthesized.

The molar volumes against the reported composition for the *fcc* phase are shown in **Fig. 1**. The red line represents the volume increase generally observed for transition metal–hydrogen systems, i.e. approximately 2.0 Å³ per hydrogen atom [53]. For H/Cr = 0, the value 7.50 × 10⁻⁶ m³/mol corresponding to a calculated metastable *fcc* Cr is taken from Li et al. [54]. The plain symbols in **Fig. 1** represent the experimental values [30,42–44,46,47,49,50]. It can be seen that the cell parameter remains close to 3.85 ± 0.01 Å [30,42–44,46,47,49,50] whatever the supposed

hydrogen content in contradiction with the usual behavior represented by the red line, **Fig. 1** and **Table 3**. Moreover, these experimental points are in accordance with the red line, only if the composition is close to 1 H/M which is therefore probably the real composition of all these samples. Furthermore, the tendency shown by the red line is supported by the density functional theory (DFT) calculations on the two prototypes. The volume obtained for the CaF₂ prototype is 4.01 Å [55], 4.101 Å [56] and 4.085 Å, this work. Regarding the rock salt structure, the volume obtained is 3.71 Å [55], 3.797 Å [56] and 3.779 Å, this work. The cell parameters calculated in the CaF₂-type structure is much larger than the experimental cell parameters found, i.e., 3.85 - 3.86 Å.

Possible explanations for errors in the composition evaluation can be that during the electrochemical preparation, H₂ bubbles can be trapped or even H₂ bubbles can be liberated during the synthesis (competitive reaction) or that the accuracy of the determination technique is deficient due to lack of precision of the equipment itself or due to poor calibration.

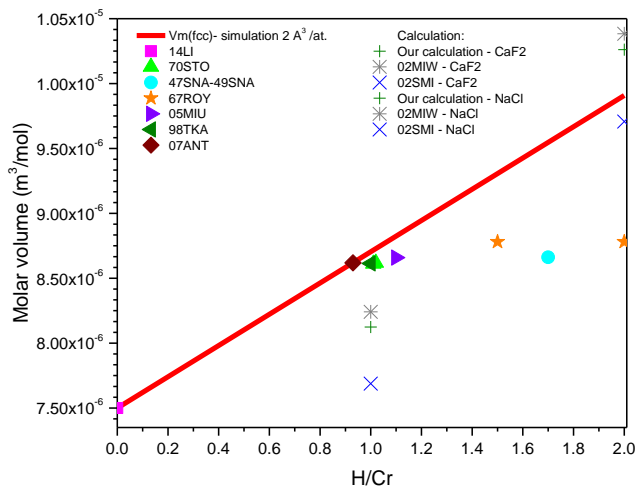


Fig. 1 – Molar volume against the atomic ratio for the *fcc* phase. The red line represents the expected change of volume induced by hydrogen, i.e. 2.0 \AA^3 by atom of metal [53]. Experimental data are from Snavely [49], Snavely and Vaughan [50], Roy and Gibb [43], Stock and Hardcastle [44], Tkacz [30], Miura et al. [46], Antonov et al. [47], Li et al. [54]. Calculated data are from Miwa and Fukumoto [56], Smithson et al. [55] and this work.

Finally, Antonov et al. [47], performed neutron diffraction on the *fcc* hydride. They showed and proved that the hydride is $Fm\bar{3}m$. They tested octahedral and tetrahedral occupancies in the structure refinement and claimed unambiguously that hydrogen is located in the octahedral site.

As a conclusion, it is assumed that the *fcc* hydride has the NaCl-type structure with the hydrogen located in the octahedral site and that the composition is 1 H/Cr. It is worth to mention that this hydride has the same composition as the *hcp* hydride.

Table 4 – Experimental phase diagram and thermodynamic data on the Cr–H system.

Phase(s)	Data type	Range	Technique	Reference	Used
<i>bcc</i>	Hydrogen solubility data	720-1405 K	Sieverts	[57]	Yes
	at $p=10^5$ Pa	770-1485 K	Sieverts	[58]	Yes
		770-1400 K	Extraction	[59]	Yes
		1020-1620 K	Extraction	[60]	Yes
		875-1805 K	Extraction	[61]	Partly yes
<i>hcp</i>	$\Delta_f H_{hcp-CrH}^\circ$ (obtained from decomposition) at $p=10^5$ Pa	298 K	Calorimetry	[62]	Comp ^a
	$\Delta_f H_{hcp-CrH}^\circ$ (obtained from decomposition) at $p=10^5$ Pa	298 K	Calorimetry	[63]	Comp ^a
	$\Delta_f H_{hcp-CrH}^\circ$	298 K	Derived from hydride formation	[45]	Comp ^a

	at $p=10^5$ Pa		pressure		
	S_f^0	298 K	Heat capacity	[64]	No
	at $p=10^5$ Pa				
	Hydrogen solubility				
<i>liquid</i>	data	2176 K	Sieverts	[65]	Yes
	at $p=10^5$ Pa				
	Melting				
<i>liquid-bcc</i>	temperature as a	2135-2176 K	<i>in situ</i> laser		
	function of	0.1-15 MPa	speckle	[66]	Yes
	hydrogen pressure				
	p - C - T	423 K	Resistivity and		
<i>bcc-hcp</i>	formation	172-348 MPa	Sieverts	[45,67]	Partly yes
		425-650 K	Resistivity and		
		317-424 MPa	Sieverts	[68]	No
	p - C - T	423 K	Resistivity and		
	decomposition	320 MPa	Sieverts	[9,45,69]	Yes
		240-690 K	Resistivity and		
		317-424 MPa	Sieverts	[68]	Yes
	p - T phase diagram	273-1500 K	hp SXR		
<i>bcc-hcp</i>		0-120 GPa	RD	[11]	Comp ^a
	p - C - T	423 K	Sieverts		
<i>bcc-fcc</i>	decomposition	0-0.8 GPa		[30]	Yes
	p - T phase diagram	273-1400 K	hp SXR		
<i>bcc-hcp- fcc-liquid</i>		0-5.5 GPa	RD	[10]	Partly yes

^a Comp: only for comparison.

The hydrogen solubility in the *bcc* phase was measured using Sieverts apparatus [30,57,58], resistivity measurement [67] or extraction technique [59–61]. All the authors [57–60] agree on the increase of the hydrogen solubility as a function of temperature with the exception of Shapovalov et al. [61] at low temperature, reason for which these measurements were excluded. The solubility of hydrogen in the liquid phase was only measured by Weinstein and Elliott [65].

Few authors have studied the pressure–composition isotherms [45,67]. A hysteresis of few kilobars is observed between the absorption and decomposition of the hydrides CrH.

The high pressure and high temperature phase diagrams were measured from ambient temperature to 1500 K over a large range of pressure [10,11,68]. Fukai and Mizutani [10] have studied the phase stability up to 1300 K and 6 GPa. The *hcp* phase is stable at high pressure and at relatively high temperature. Above 1000 K, a *fcc* phase is stabilized until up to melting.

The gas-eutectic equilibrium, namely solid–liquid–gas equilibrium, has been studied by Shapovalov et al. [61] over a pressure range from 0.010 to 1.5×10^7 Pa by thermal analysis technique.

The enthalpy of desorption at 298 K has been measured using calorimetry by Sieverts and Gotta [62] and Randzio and Bojarski [63] for the hexagonal monohydride. They found respectively -7.95 kJ/mol–H for \sim CrH_{0.22} and an average value of - 8.01 kJ/mol–H for hydrides ranging from CrH_{0.37} to CrH_{0.49}. Baranowski et al. [45,67] have derived and extrapolated at room temperature the enthalpy from hydride equilibrium pressure for *hcp*–CrH and found -7.55 ± 1.30 kJ/mol–H. Furthermore, the enthalpy of formation of *fcc* hydride extracted from the plateau pressure is -7.301 kJ/mol–H. [30].

3. CALCULATION METHOD

3.1 Ab-initio calculations

DFT calculations were carried out using the generalized gradient approximation (GGA) with the Perdew-Burke-Ernzerhof (PBE) [70] functional, using the Vienna Ab-initio Simulation Package (VASP) [71,72]. The pseudopotential including 12 valence electrons was considered for Cr (i.e. including the *p*-pseudocore electrons). An energy cutoff of 600 eV with spin polarization was used for the plane wave basis set. For each phase considered, a highly dense grid of k-points in

the irreducible wedge of the Brillouin zone was generated with the Monkhorst-Pack scheme [73], e.g. 21x21x21 for cubic CrH leading to 286 unique k-points spaced by less than 0.05 Å⁻¹. All these parameters ensured good convergence for the total energy.

The heat of formation of every hydride at 0 K was calculated from the difference between total energies of the considered hydride and those of pure antiferromagnetic Cr and of the dimer H₂ molecule in a box according to:

$$\Delta_f H_{CrH_x} = E_{CrH_x} - E_{Cr} - \frac{x}{2} E_{H_2} \quad (1)$$

The formation energy $\Delta_f H_{CrH_x}$ was corrected by the zero-point energy (ZPE). This energy was determined from the phonon branches obtained by the calculation in the harmonic approximation (HA): $E^{ZPE} = \frac{1}{2} \sum_i \hbar \omega_i$ assuming that every ω_i is not an imaginary frequency.

The HA-phonon calculations were performed using the supercell approach [74]: from a fully relaxed structure within inter-atomic forces under 10⁻⁸ eV.Å⁻¹, supercells of size larger than 7 Å of length vector with relevant atomic displacements were then built using the Phonopy code [75]. After the determination of resulting inter-atomic forces, the Phonopy code was used to determine from the set of forces, the frequencies of the eigenmodes of vibration.

In addition to HA calculation, quasiharmonic approximation calculations (QHA) have been considered. In the frame of the QHA, this above procedure was repeated for several cell volumes in order to include the pressure dependence of the eigenmodes. QHA-phonon calculations were carried out to calculate the temperature dependence of the volume, the thermal expansion coefficient and the bulk modulus of Cr and its hydrides.

3.2. Thermodynamic modeling

The Cr and Cr–H systems have been assessed with the Calphad method using the PARROT module [76] in the Thermo-Calc software package [77]. The assessment consists in describing the Gibbs energies of all the phases of the system by equations with parameters adjusted with a least square algorithm minimizing the difference between experimental or theoretical, and calculated data. The experimental data are carefully selected after the complete review made in section 2.

The thermodynamic properties of multicomponent systems may be predicted by extrapolation. This extrapolation is made putting together all the terms of the Gibbs energy of the sub-systems. In this work, the descriptions of the three binary systems Cr–H (this work), H–Zr [78] and Cr–Zr [79] are extrapolated to construct the Cr–H–Zr system in order to predict the properties of *bcc* $\text{Cr}_x\text{Zr}_{1-x}$ alloys with hydrogen without any ternary parameter.

3.2.1 Gas phase.

Both species, chromium and dihydrogen are considered for the gas modeling. The Gibbs energy of chromium and di-hydrogen at $p = 10^5$ Pa were extracted from the SSUB [80] and PURE databases [81]. As the modeling of this system involved high pressure data, the nonideality of the di-hydrogen needs to be considered using an equation developed by Joubert [82]. At high pressure, the molar volume of the gaseous chromium was chosen to converge towards the molar volume of the solid chromium. No interaction is considered between chromium and dihydrogen.

3.2.2 Liquid phase.

In this optimization, the liquid phase is described using a two-sublattice model [83] with the formula $(\text{Cr})_1:(\text{H}, \text{Va})_1$. This choice of an interstitial rather than a substitutional model is motivated by the possible compatibility with other metal–hydrogen systems [84,85] using the same model. More explanation can be found in the reference [86].

3.2.3 Solid phases.

The model used to describe the *bcc* solid phase is a two-sublattice model [83] with $(\text{Cr})_1:(\text{H}, \text{Va})_3$, i.e. chromium fully occupies the *bcc* host lattice represented by the first sublattice, hydrogen and vacancies occupy the tetrahedral interstitial sites represented by the second sublattice. The reason of the choice of a multiplicity of 3 for the interstitial site is as follows. In principle, the number of interstitial tetrahedral sites in the *bcc* structure is 6 per metal atom. However, because of the H–H proton repulsions [86], H atom cannot occupy two neighbor sites simultaneously. Thus, the multiplicity was set to 3 H for 1 Cr in our model. The Gibbs energy is described in section 3.2.4.

The model used to describe the hydride phases is a stoichiometric model [83] with $(\text{Cr})_1:(\text{H})_1$ for the *hcp* and *fcc* phases. Both *hcp* and *fcc* phases have a complete occupancy of hydrogen in

the octahedral site. This description is selected due to lack of convincing data regarding the non-stoichiometry of the phases versus temperature and pressure. The Gibbs energy is described in section 3.2.4.

3.2.4 Gibbs energy of the liquid and solid phases.

3.2.4.1 Gibbs energy of the hydrides.

The hydride phases, *hcp* and *fcc*, are modeled as stoichiometric phases, thus the Gibbs energy is described as follows:

$$G^\Phi = G_{Cr}^{bcc} + \frac{1}{2} G_{H_2}^{SER} + a^\Phi + b^\Phi T + {}^{phys}G^\Phi \quad (\Phi = hcp \& fcc) \quad (2)$$

With ${}^{phys}G^\Phi$ is the physical Gibbs energy. The Gibbs energy of chromium was taken from PURE database [81]. The physical contribution ${}^{phys}G^\Phi$ will be described in the section 3.2.4.3.

3.2.4.2 Gibbs energy of the liquid and bcc phases.

The Gibbs energy for the liquid and the *bcc* phases is described below:

$$G^\Phi = {}^{ref}G^\Phi + {}^{id}G^\Phi + {}^{ex}G^\Phi + {}^{phys}G^\Phi \quad (\Phi = liquid, bcc) \quad (3)$$

With ${}^{ref}G^\Phi$, ${}^{id}G^\Phi$ and ${}^{ex}G^\Phi$ represent the reference Gibbs energy, the ideal Gibbs energy, and the excess Gibbs energy, respectively.

The first three terms are expressed below:

$${}^{ref}G^\Phi = y_{VA} G_{Cr:VA}^\Phi + y_H G_{Cr:H}^\Phi \quad \text{for } liquid \& bcc \quad (4)$$

$${}^{ref}G^\Phi = y_{VA} G_{Cr:VA}^\Phi + y_H \left(G_{Cr}^\Phi + \frac{X}{2} G_{H_2}^{SER} + a^\Phi + b^\Phi T \right) \quad \text{for } liquid \& bcc \quad (5)$$

$${}^{id}G^\Phi = XRT \left[\sum_{i=H,VA} y_i^\Phi \ln(y_i^\Phi) \right] \quad \text{for } liquid \& bcc \quad (6)$$

$${}^{ex}G^\Phi = y_H y_{VA} \sum_{i=0}^n L_{Cr:VA,H}^{i,\Phi} (y_H - y_{VA})^i \quad \text{for } liquid \& bcc \quad (7)$$

With $X = 1$ for the liquid phase and $X = 3$ for the *bcc* phase. The Gibbs energy of chromium is taken from the PURE database [81]. y_{VA} and y_H are site-fractions of vacancies and hydrogen, respectively.

The interaction parameters $L_{Cr:VA,H}^{i,\Phi}$ can be expressed as a function of temperature:

$$L_{Cr:VA,H}^{i,\Phi} = c^{i,\Phi} + d^{i,\Phi}T \quad (8)$$

In equations (2), (5) and (8) are shown the parameters to be optimized, i.e. a^Φ , b^Φ , $c^{i,\Phi}$, $d^{i,\Phi}$.

The physical contribution $^{phys}G^\Phi$ will be described in the next section.

3.2.4.3 Physical Gibbs energy.

The last Gibbs energy term to describe is the physical contribution $^{phys}G^\Phi$. Here the liquid and solid phases were split apart, and the equation is given by

$$^{phys}G^{liquid} = \Delta G_m^{liquid}(T, p) \quad (9)$$

$$^{phys}G^\Phi = ^{magn}G^\Phi + \Delta G_m^\Phi(T, p) \quad (\Phi = bcc, hcp \text{ or } fcc) \quad (10)$$

The magnetic contributions of the solid phases to the total Gibbs energy were described using the model of Hillert–Jarl–Inden [87,88]:

$$^{magn}G^\Phi = RT \ln(\beta + 1) g(\tau) \quad (11)$$

where R is the gas constant, β is the Bohr's magnetons per mol of atoms and τ is T/T_C . T_C is the magnetic ordering temperature and $g(\tau)$ is a polynomial function. For the solid solution phases T_C and β are composition dependent.

The last contribution is the temperature and pressure dependence for the molar Gibbs energy $\Delta G_m^\Phi(T, p)$ related to the changes of volume. In this assessment, relatively high pressure is considered (tens of GPa). Thus, the use of a modified equation of state proposed by Lu et al. [12] based on the EOS of Grover [89] is necessary to avoid inconsistencies in the pressure–temperature phase diagram. The following equations were expressed:

$$\Delta G_m^\phi(T, p) = \int_{p_0}^p V_m(T, p) dp \quad (12)$$

$$V_m(T, p) = c(T) E_i^{-1} \left[E_i \left(\frac{V_m(T, p_0)}{c(T)} \right) + (p - p_0) \kappa(T, p_0) \exp \left(-\frac{V_m(T, p_0)}{c(T)} \right) \right] \quad (13)$$

Here, the 0 subscript symbol stands for the reference state at 1 bar, $c(T)$ is a pressure fitting parameter, $\kappa(T, p_0)$ is the isothermal compressibility at 1 bar, $E_i = \int_z^\infty \frac{e^{-x}}{x} dx$ is the exponential integral function and E_i^{-1} the inverse function. The molar volume at 1 bar, $V_m(T, p_0)$, is given by:

$$V_m(T, p_0) = V_0 \exp \left(\int_{T_0}^T 3\alpha dT \right) \quad (14)$$

Here, V_0 is the molar volume at a reference temperature T_0 and 1 bar and 3α stands for the volumetric thermal expansion.

In Thermo-Calc software, the terms of equations 13 and 14 $\int_{T_0}^T 3\alpha dT$, $\kappa(T, p_0)$, $c(T)$ and V_0 are incorporated as functions V_A , V_K , V_C and V_0 respectively. The three first functions are dependent on both temperature and composition and the latter, V_0 only depends on composition. Explanations can be found in the **Table 5** where V_{XX} are the fitted parameters. Recently, Joubert et al. [13] improved the model proposed by Lu et al. [12] using an exponential contribution to avoid inconsistencies, for instance negative C_p , at relatively high pressure.

Table 5 – Functions and parameters used for the compressibility.

Function	Unit	Meaning
$V_0 = V_{10}$	$\text{m}^3 \cdot \text{mol}^{-1}$	Volume at a reference temperature T_0 and 1 bar
$V_A = V_{11} T \exp(-p/p_{cut})$ $+ V_{12} T^2 \exp(-p/p_{cut})$ $+ V_{13} \ln(T)$ $+ V_{14} T^3 \exp(-p/p_{cut})$	-	Integrated thermal expansion
$V_C = V_{15} + V_{16} T \exp(-p/p_{cut})$	Pa^{-1}	Function to fit high pressure data

$V_K = V_{17} + V_{18} T \exp(-p/p_{cut})$ $+ V_{19} T^2 \exp(-p/p_{cut})$	$m^3 \cdot mol^{-1}$	Isothermal compressibility at 1 bar
--	----------------------	--

Finally, using the previous equations, a rearrangement can be made:

$$V_m(T, p) = V_C E_i^{-1} \left[E_i \left(\frac{V_0 \exp(V_A)}{V_C} \right) + (p - p_0) V_K \exp \left(-\frac{V_0 \exp(V_A)}{V_C} \right) \right] \quad (15)$$

4. RESULTS AND DISCUSSION

This section is divided into three parts. First, the contribution to the molar Gibbs energy from the molar volume data of each phase, $\Delta G_m^\Phi(T, p)$, is treated. Secondly, the complete assessment of the binary Cr–H system is presented. Finally, the robustness of our model is tested by comparing hydrogenation measurements made on a binary Cr–Zr alloy to predictions made using our database.

4.1. Temperature and pressure dependence of the volume data for the molar Gibbs energy, $\Delta G_m^\Phi(T, p)$.

4.1.1. Pure Cr.

In this section, the results for the stable end members of the *bcc* Cr and liquid chromium are displayed. The temperature and pressure dependence of the volume data for the molar Gibbs energy were refined using only experimental data. Thus, the phonon and DFT calculated data were not used as they systematically underestimate the volume, thermal expansion, and bulk modulus. Trials with other functional like PBEsol [90] have been made, but the results were worse than with the PBE, so that, only the PBE functional was used. Moreover, this phenomenon has been observed in previous studies and our calculations are in good agreement with previous papers [11,91]. The results can be found in the **Fig. 2** to **Fig. 6** and in the **Table 7**.

Thermal expansion is adjusted with a linear model and thus is not described properly down to very low temperature (it does not converge to zero as phonon data does). The magnetic contribution to the Gibbs energy is considered (see above). However, the effect of magnetism on volume properties, seen for example by the decrease of the bulk modulus at the Néel temperature is not considered.

A choice has been made in order to describe the most accurately as possible the molar volume of the liquid with the temperature, **Fig. 6**, and the melting temperature versus the pressure, **Fig. 3**. The Clapeyron equation:

$$\frac{dT_m}{dp} = \frac{\Delta V_m}{\Delta S_m} \quad (16)$$

with ΔV_m is the melting volume and ΔS_m is the melting entropy, shows the dependence between the molar volume and the melting temperature. It was impossible to fit simultaneously and properly T_m against the pressure, **Fig. 3**, and the molar volume against temperature, **Fig. 2**, of the liquid due to this equation. We made a compromise with a more important weight was considered for the data of Errandonea et al. [38].

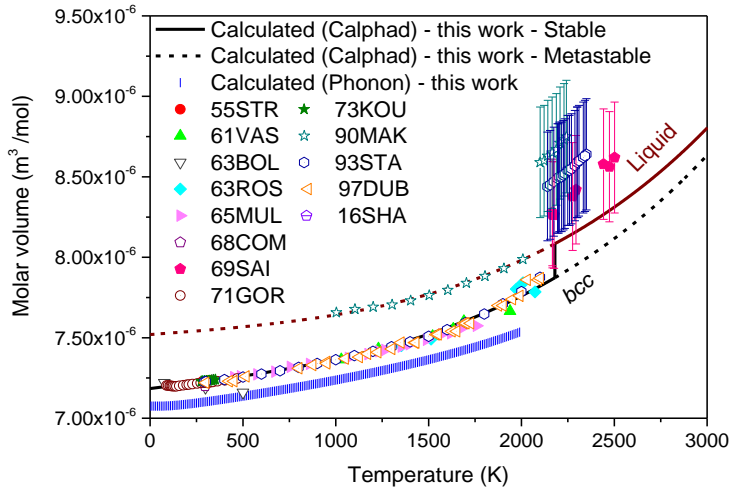


Fig. 2 – Calculated molar volume of *bcc* and liquid Cr as a function of temperature. Experimental data are from Straumanis and Weng [14], Vasyutinskii et al. [15], Bolef and De Klerk [16], Ross and Hume-Rothery [17], Muller and Dunner [18], Combley [19], Gordienko and Nikolaev [20], Koumelis [21], Makeev and Popel [22], Stankus [23], Dubrovinskaia et al. [24], Saito et al. [37]. Phonon calculation is from this work.

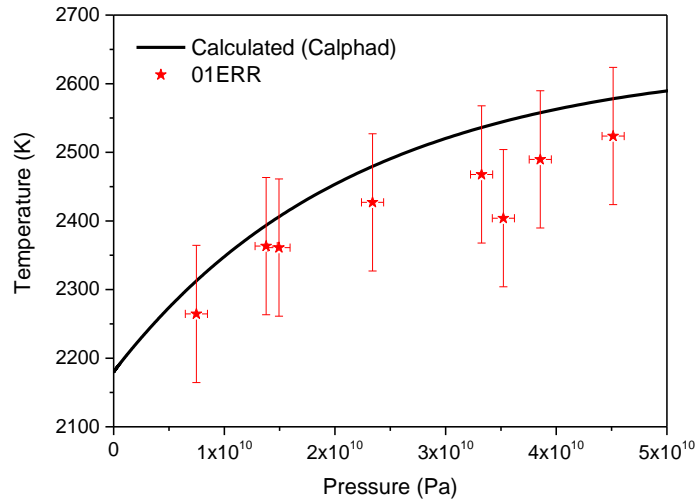


Fig. 3 – Calculated melting curve of Cr. Experimental data is from Errandonea et al. [38].

A good agreement is found, as shown in **Fig. 4** to **Fig. 6**, between the model for the *bcc* Cr and the experimental values within the temperature and pressure range allowed in this model.

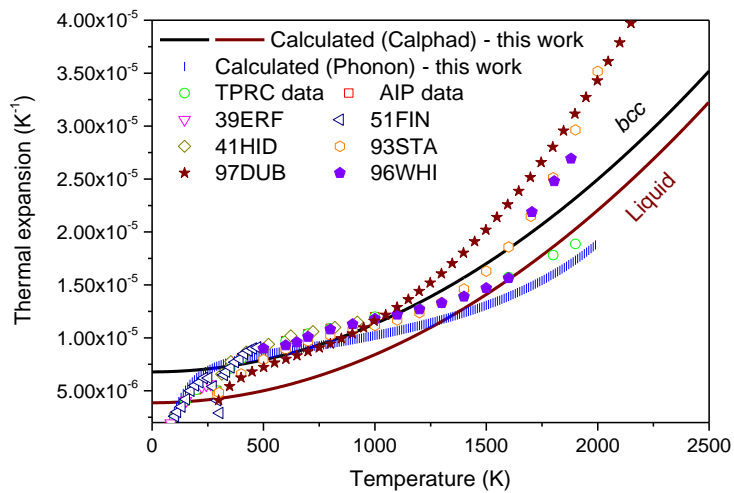


Fig. 4 – Calculated thermal expansion of *bcc* and liquid Cr as a function of temperature. Experimental data for *bcc* Cr are from Erfling [25], Hidnert [26], Fine et al. [27], Stankus [23], White and Andrikidis [28] and Dubrovinskaia et al. [24]. Phonon calculation is from this work.

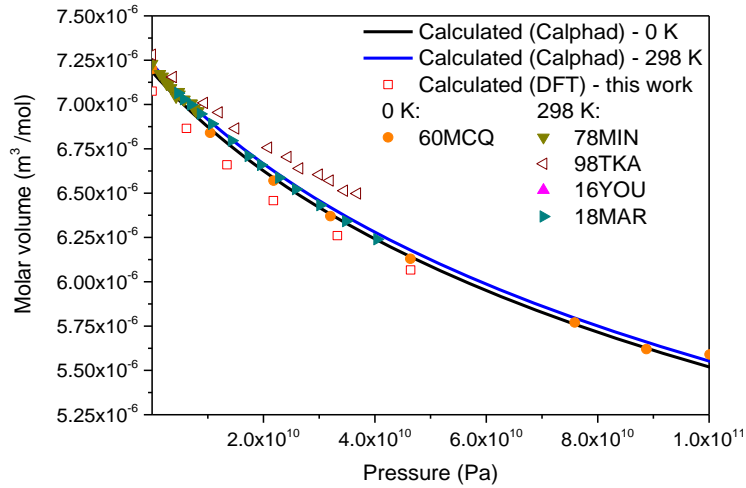


Fig. 5 – Calculated molar volume of *bcc* Cr as a function of pressure. Experimental data are from McQueen and Marsh [36], Ming and Manghnani [29], Tkacz [30], Young et al. [31], Marizy et al. [11]. DFT calculations are from this work.

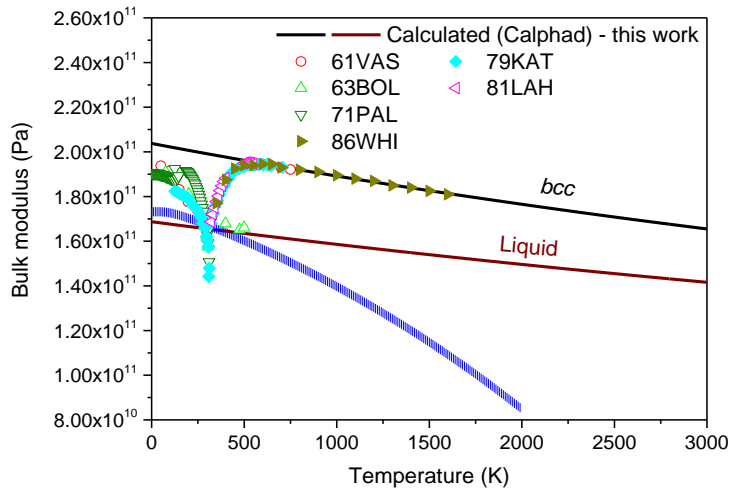


Fig. 6 – Calculated bulk modulus of *bcc* and liquid Cr as a function of temperature. Experimental data are from Bolef and De Klerk [16], Palmer and Lee [32], Katahara et al. [33], Lahtenkorva and Lenkkeri [34] and White et al. [35]. Phonon calculation is from this work.

4.1.2 Cr:H end members.

In this section, the description of the temperature and pressure dependence of the volume data of the Cr:H end members is displayed, i.e. *bcc* CrH₃, liquid CrH, *fcc* CrH and *hcp* CrH.

The molar volume $V_{Cr:VA}^{0,bcc}$ was optimized at a value of $7.1846 \times 10^{-6} \text{ m}^3/\text{mol}$. The usual volume change induced by hydrogen absorption is $1.746 \times 10^{-6} \text{ m}^3/\text{mol}$ per hydrogen atom [53]. The value for the cubic CrH₃ molar volume $V_{Cr:H}^{0,bcc}$ was set to the calculated DFT value, i.e. $1.228 \times 10^{-5} \text{ m}^3/\text{mol}$, in line with this expected increase. The other *bcc* Cr:H functions, i.e. V_A , V_C and V_K were set to the same values as the ones found for Cr:VA *bcc* end member assuming that the hydrogen does not affect the physical properties.

A good approximation is to consider that the coordination in the liquid phase is similar to that in the *bcc* phase; thus, the molar volume V_0 of the liquid end member CrH was estimated equal to the molar volume of solid CrH, multiplied by the *hcp* / *bcc* compressibility ratio. The other functions for liquid Cr:H, i.e. V_A , V_C and V_K were fixed to the same values as the liquid end member Cr:VA. A sketch of all the molar volume versus the hydrogen content of all the end members can be found in **Fig. 7**.

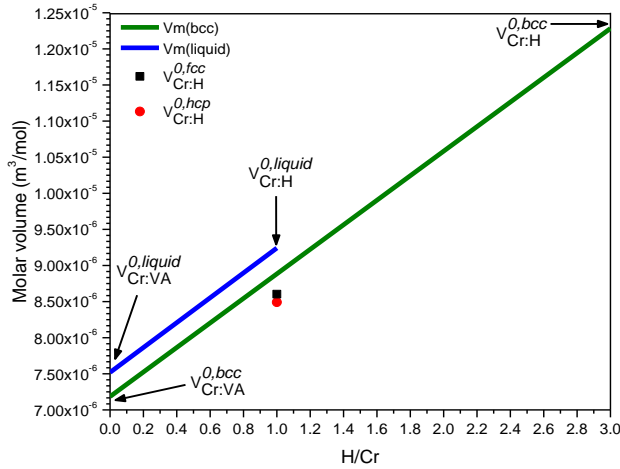


Fig. 7 – Molar volume (per mole of compound) of the end members found after optimization against H / Cr ratio.

The functions V_0 and V_C of the end member Cr:H for *fcc* phase were refined using only experimental data for the molar volume against temperature and pressure, **Fig. 8** and **Fig. 9** respectively. Ab-initio calculation were used for the thermal expansion and bulk modulus against

temperature, functions V_A and V_K , since no reliable experimental data were found in the literature, see **Fig. 10** and **Fig. 11**, respectively.

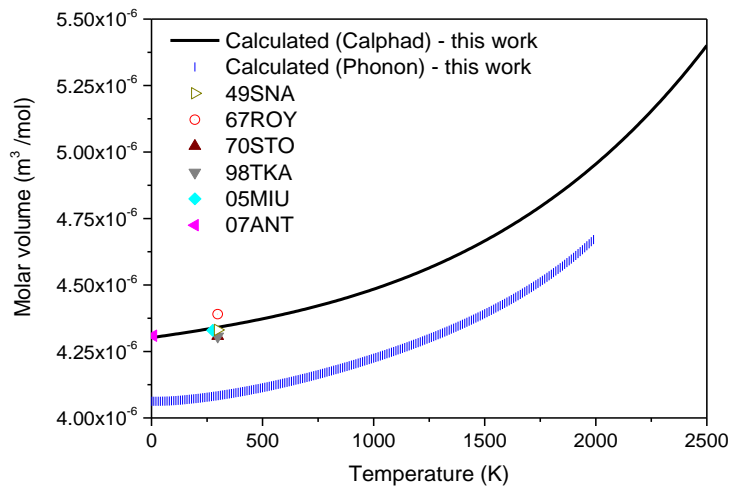


Fig. 8 – Calculated molar volume of *fcc* CrH phase as a function of temperature. Experimental data from Snaveley and Vaughan [50], Roy and Gibb [43], Stock and Hardcastle [44], Tkacz [30], Miura et al. [46], Antonov et al. [47]. Phonon calculation is from this work.

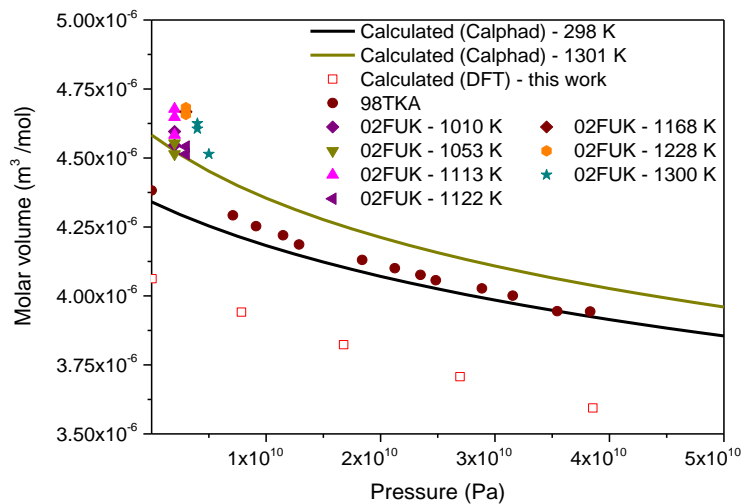


Fig. 9 – Calculated molar volume of *fcc* CrH phase as a function of pressure. Experimental data are from Tkacz [30], Fukai and Mizutani [10]. Phonon calculation is from this work.

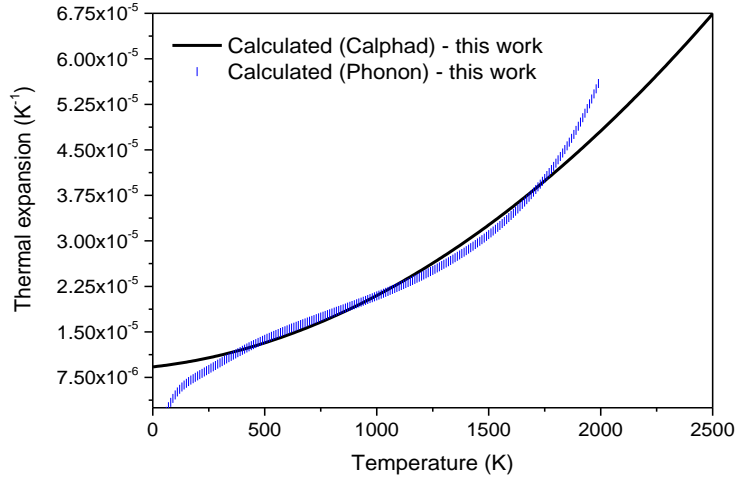


Fig. 10 – Calculated thermal expansion of *fcc* CrH phase as a function of temperature. Phonon calculation is from this work.

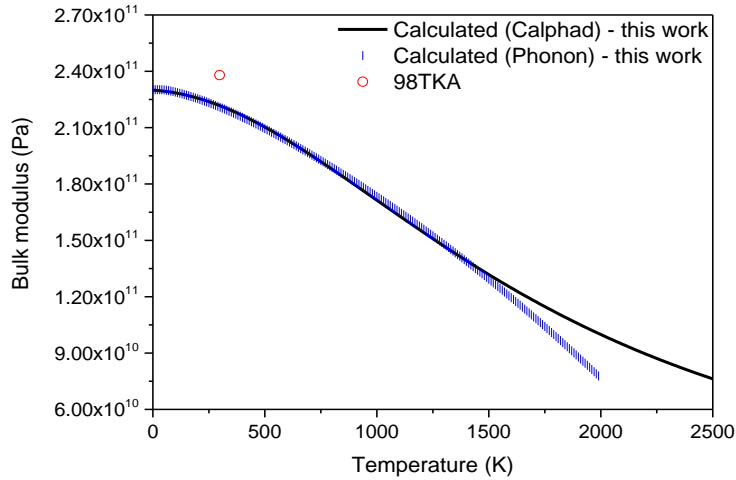


Fig. 11 – Calculated bulk modulus of *fcc* CrH phase as a function of temperature. Experimental data are from Tkacz [30]. Phonon calculation is from this work.

The results for the *hcp* end member Cr:H are reported in **Fig. 12** to **Fig. 15** and in **Table 7**. The high-pressure functions, V_0 , V_A and V_C , for the *hcp* phase are refined using experimental data.

The bulk modulus of Tkacz [30], i.e. 240 GPa at room temperature was not considered because hydrides are generally more compressible than pure metals. The value determined by Marizy et al. [11] appears therefore to be more reasonable. Regarding the bulk modulus versus temperature,

an offset was applied to the phonon data in order to match this experimental value (so-called ‘modified phonon’ curve in **Fig. 15**).

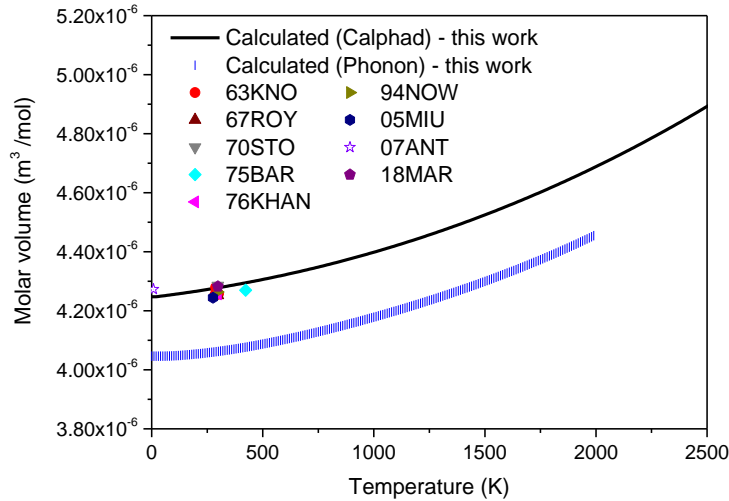


Fig. 12 – Calculated molar volume of *hcp* CrH phase as a function of temperature. Experimental data are from Knödler [42], Roy and Gibb [43], Stock and Hardcastle [44], Baranowski et al. [45], Khan and Raub [92], Nowak et al. [93], Miura et al. [46], Antonov et al. [47] and Marizy et al. [11]. Phonon calculation is from this work.

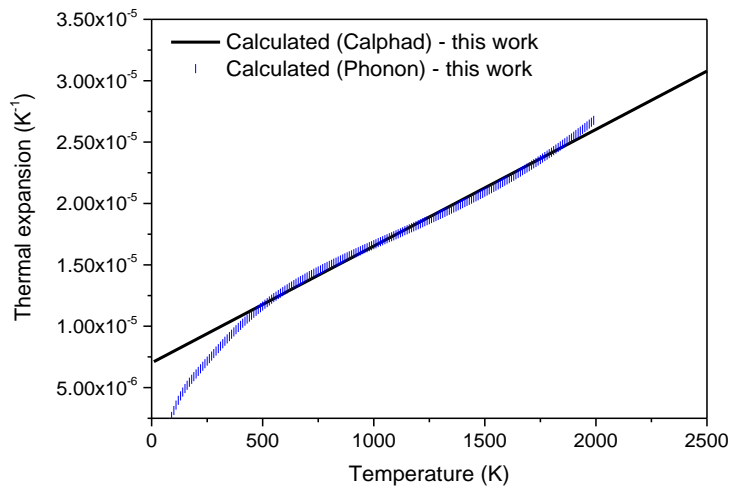


Fig. 13 – Calculated thermal expansion of *hcp* CrH phase as a function of temperature. Phonon calculation is from this work.

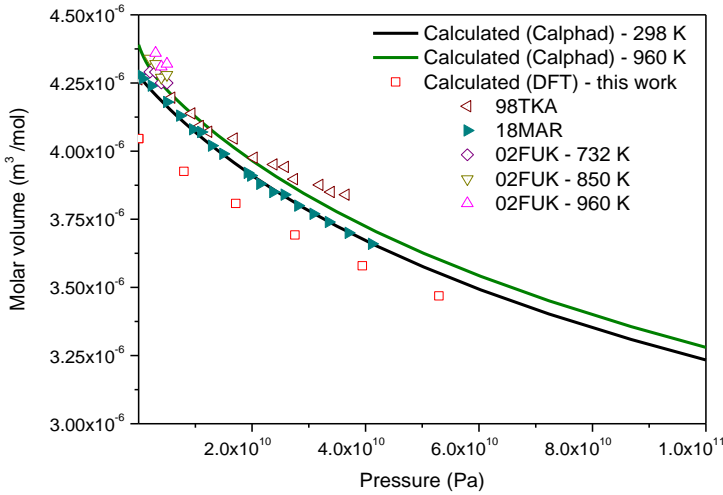


Fig. 14 – Calculated molar volume of *hcp* CrH phase as a function of pressure. Experimental data from Tkacz [30], Fukai and Mizutani [10], Marizy et al. [11]. DFT calculation is from this work.

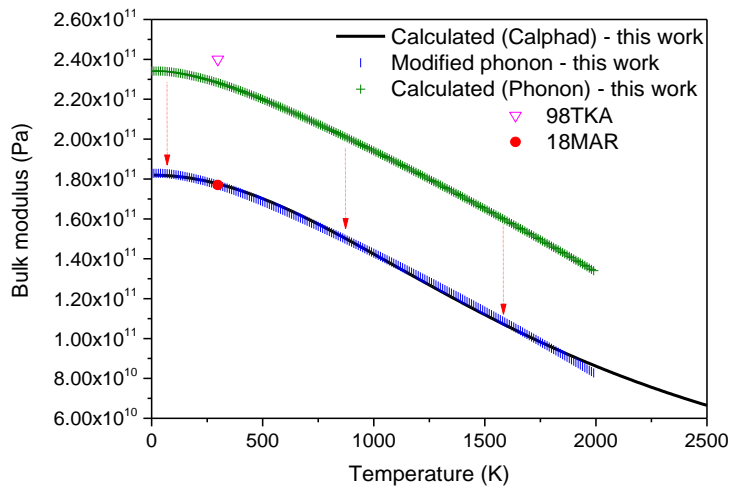


Fig. 15 – Calculated bulk modulus of *hcp* CrH phase as a function of temperature. Experimental data from Tkacz [30], Marizy et al. [11]. Phonon calculation is from this work and is adjusted to match the data from Marizy et al. [11].

4.2. Cr–H system.

Our calculated ab-initio data for the enthalpy of formation of all end members is presented in **Table 6** and they were considered as a starting point. The entropy of formation was assumed to

have the ideal value of - 65.4 J mol⁻¹ per hydrogen atom [86] corresponding to half of the entropy of di-hydrogen.

Table 6 – Calculated volume of compounds and heats of formation, $\Delta_f H$.

Formula	Phase, Structure	Volume (m ³ /mol–compound)	$\Delta_f H$ (kJ/mol–H)
CrH	<i>hcp</i> , NiAs–type	8.091 x 10 ⁻⁶	2.311
CrH	<i>fcc</i> , NaCl–type	8.124 x 10 ⁻⁶	10.142
CrH ₃	<i>bcc</i> , W–type	12.282 x 10 ⁻⁶	121.124

Regarding the Gibbs energies of the liquid and *bcc* phases, interaction parameters $L_{Cr:H,VA}^{0,liq}$ and $L_{Cr:H,VA}^{0,bcc}$ were needed. First of all, a constant interaction parameter for the liquid phase was chosen as few data were available for this phase [10,65,66]. Consequently, only three parameters were refined, two for $G_{Cr:H}^{Liq}$ and one for $L_{Cr:H,VA}^{0,liq}$, using solubility data [65] and the invariant reaction at different pressures [10,65,66]. Regarding the *bcc* phase, the interaction parameter was determined as a function of temperature and four parameters were refined (two for $G_{Cr:H}^{bcc}$ and two for $L_{Cr:H,VA}^{0,bcc}$).

Given that *hcp* and *fcc* phases have the same composition, the enthalpy and the entropy terms of $G_{Cr:H}^{hcp}$ and $G_{Cr:H}^{fcc}$ have been optimized together based on the available experimental data [9,10,30,45,68]. The latter phases will be discussed in the end of this section.

The model replicates well the isobaric data, **Fig. 16** and the eutectic solid–liquid–gas reaction, **Fig. 17**; even though, the liquid isobaric solubility data is a bit underestimated.

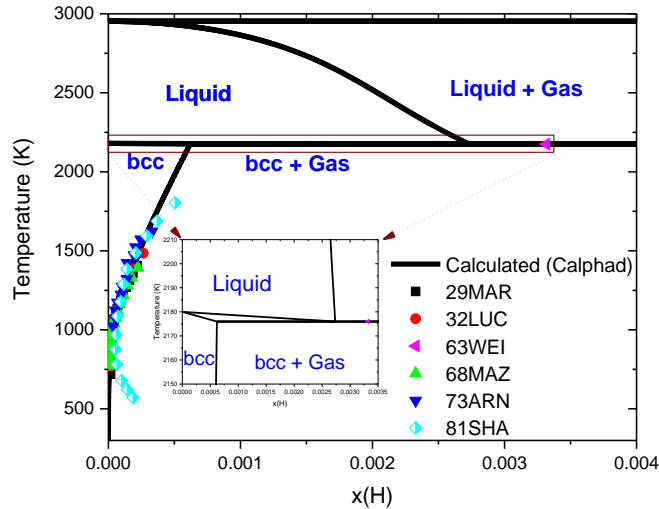


Fig. 16 – Calculated Cr–H phase diagram on the chromium rich side at ambient pressure. Experimental data are from Weinstein and Elliot [65], Martin [57], Luckemeyer-Hass and Schenck [58], Mazaev et al. [59], Arnoult and McLellan [60], Shapovalov et al. [61].

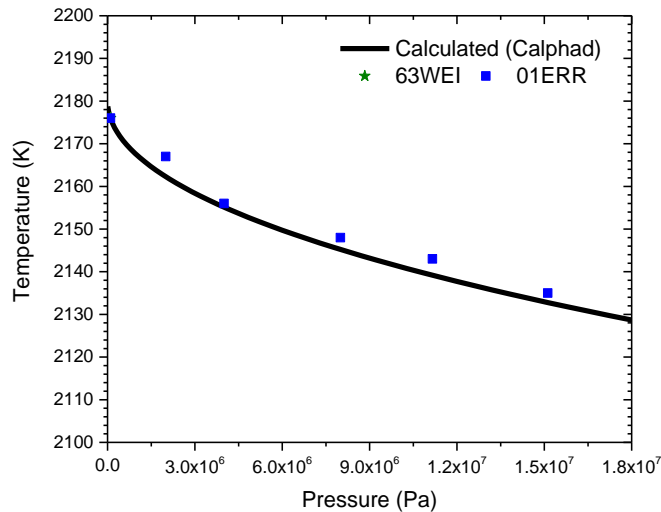


Fig. 17 – Calculated eutectic temperature as a function of pressure. Experimental data are from Weinstein and Elliot [65], Shapovalov [66].

The pressure–composition isotherm at 423 K showing the transformation of *bcc* into *hcp* phase, **Fig. 18**, is also well described regarding the plateau region. The data from Baranowski and Bojarski [67] of the *bcc* solubility branch at low hydrogen content are incompatible with the data from previous researchers [57–61] due to a high imprecision of the experimental technique. A

hysteresis of few kilobars is observed between the absorption and decomposition of the hydrides and cannot be modeled. The plateau pressure or the van't Hoff diagram, **Fig. 19**, was evaluated using the *hcp*-CrH decomposition data.

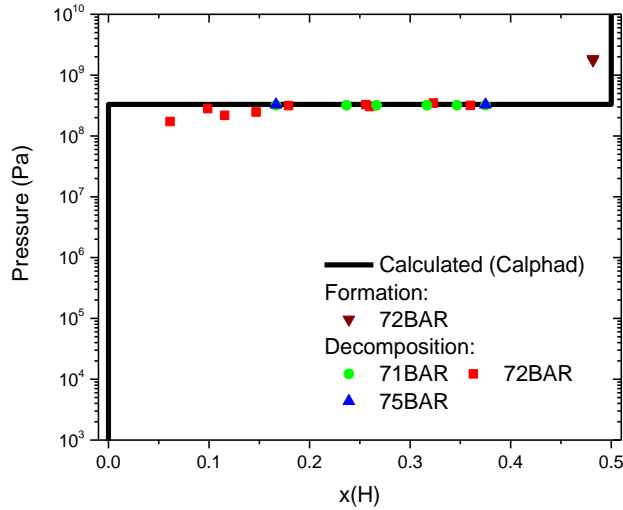


Fig. 18 – Calculated pressure–composition isotherm at 423 K. Experimental data are from Baranowski [69], Baranowski and Bojarski [9,67], Baranowski et al. [45].

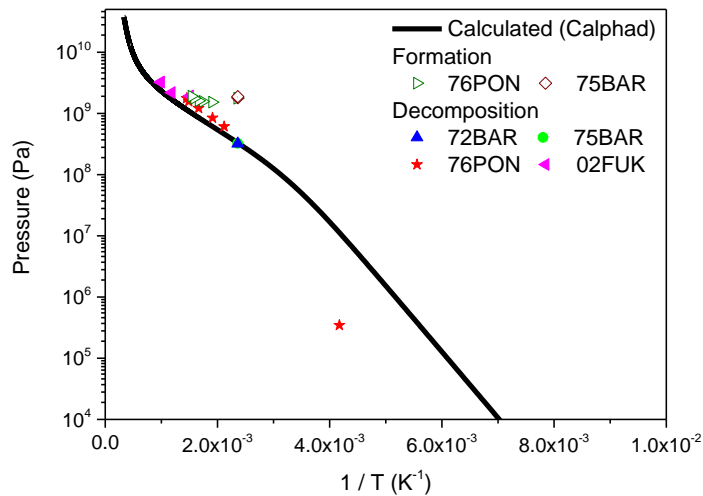


Fig. 19 – Calculated plateau pressure as a function of the inverse temperature. Experimental data are from Baranowski and Bojarski [9], Baranowski et al. [45], Poniatovskii and Belash [68], Fukai and Mizutani [10].

A delicate aspect was to reproduce the most accurately as possible the temperature–pressure phase diagram, **Fig. 20**. First of all, a recent thermodynamic study [94], using Clapeyron equation (16), has shown that the sketch of the T – p phase diagram of the paper of Fukai and Mizutani [10] and some part of this pressure–temperature phase diagram is not well constructed. Thus, during the optimization, some data from Fukai and Mizutani [10] were rejected to accommodate as well as possible all the literature data available, like, for example, the presence of the *fcc*–phase at 2 GPa and that of the *bcc* phase at 3 GPa where it is believed that the thermodynamic equilibrium was not reached.

It is worth mentioning that the plateau pressure data of **Fig. 19** can also be seen as the line between *bcc*+gas and *hcp*+gas fields in **Fig. 20**. Moreover, this assessment reproduces correctly the data from Tkacz [30] concerning the metastable *bcc*–*fcc* equilibrium pressure at 423 K. This can be seen by extrapolating, in the **Fig. 20**, the line between *bcc* + gas and *fcc* + gas down to 400 K.

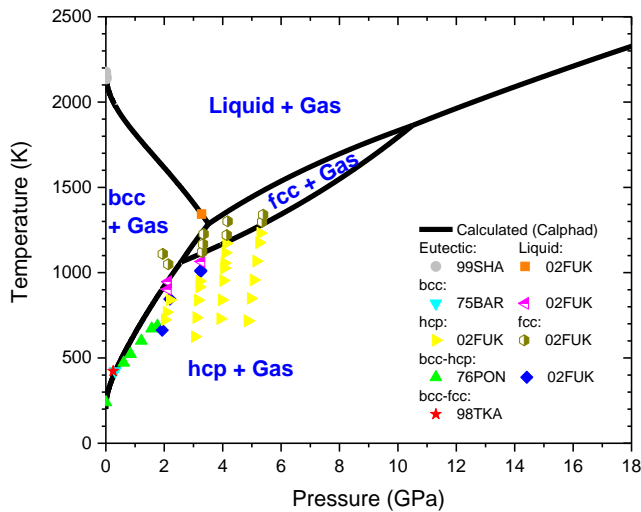


Fig. 20 – Calculated temperature–pressure phase diagram. Experimental data are from Baranowski et al. [45], Poniatovskii and Belash [68], Tkacz [30], Shapovalov [66], Fukai and Mizutani [10].

As seen in **Fig. 20**, the *fcc* phase appears above 2 GPa, this is highlighted by plotting the phase diagram at 2 GPa and 3 GPa, **Fig. 21** and **Fig. 22**, respectively.

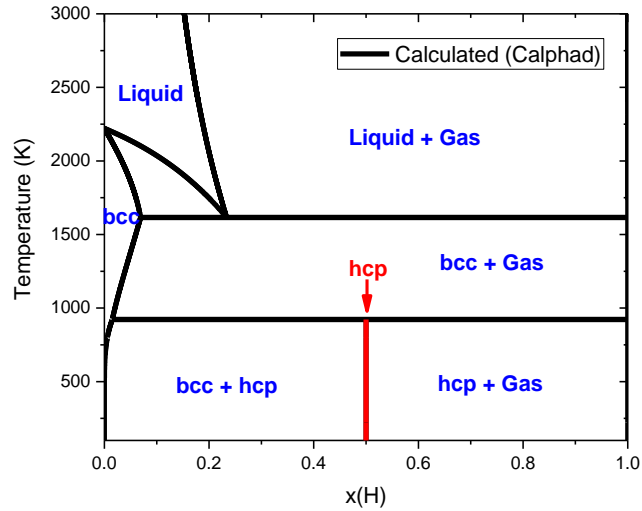


Fig. 21 – Calculated Cr–H phase diagram at 2 GPa.

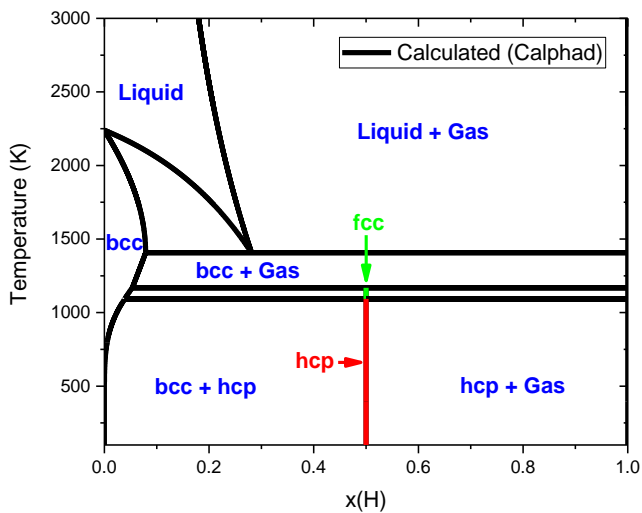


Fig. 22 – Calculated Cr–H phase diagram at 3 GPa.

The reliability of the temperature–pressure phase diagram assessed was also validated by the value of the Gibbs energy found for the hydride phases, **Table 7**, where the *hcp* phase is found more stable than the *fcc* phase as expected from literature review, see section 2.3 and ab-initio calculations.

Table 7 – Optimized thermodynamic parameters for the Cr–H system.

Phase	Parameter	Value (G and L in $\text{J}\cdot\text{mol}^{-1}$, p in Pa, V^0 and V^C in $\text{m}^3\cdot\text{mol}^{-1}$, V^K in Pa^{-1})
-------	-----------	--

	p_{cut}	1×10^{-9}
	$p_{cut'}$	1×10^{-12}
	$G_{H_2}^{Gas}$	see ref [86]
gas	G_{Cr}^{Gas}	$G_{Cr}^{Gas,SER} + RT \ln p + 7.1846 \times 10^{-6} p - 7.1846 \times 10^{-1}$
	$G_{Cr:H}^{Liq}$	$G_{Cr}^{SER} + \frac{1}{2} G_{H_2}^{SER} - 7.952 \times 10^3 + 6.540 \times 10^1 \times T$
	$L_{Cr:H,VA}^{0,liq}$	-2.7890×10^4
	$V_{Cr:VA}^{0,liq}$	7.5200×10^{-6}
	$V_{Cr:VA}^{A,liq}$	$1.1608 \times 10^{-5} T \exp\left(-\frac{p}{p_{cut'}}\right) + 4.5466 \times 10^{-12} T^3 \exp\left(-\frac{p}{p_{cut}}\right)$
	$V_{Cr:VA}^{C,liq}$	1.5202×10^{-6}
liquid	$V_{Cr:VA}^{K,liq}$	$5.9269 \times 10^{-12} + 3.7849 \times 10^{-16} T \exp\left(-\frac{p}{p_{cut}}\right)$
	$V_{Cr:H}^{0,liq}$	9.2421×10^{-6}
	$V_{Cr:H}^{A,liq}$	$1.1608 \times 10^{-5} T \exp\left(-\frac{p}{p_{cut'}}\right) + 4.5466 \times 10^{-12} T^3 \exp\left(-\frac{p}{p_{cut}}\right)$
	$V_{Cr:H}^{C,liq}$	1.5202×10^{-6}
	$V_{Cr:H}^{K,liq}$	$5.9269 \times 10^{-12} + 3.7849 \times 10^{-16} T \exp\left(-\frac{p}{p_{cut}}\right)$
	$G_{Cr:H}^{bcc}$	$G_{Cr}^{SER} + \frac{3}{2} G_{H_2}^{SER} + 1.2065 \times 10^5 + 1.9620 \times 10^2 T$
	$L_{Cr:H,VA}^{0,bcc}$	$-3.7280 \times 10^3 - 3.8378 \times 10^1 T$
	$V_{Cr:VA}^{0,bcc}$	7.1846×10^{-6}
bcc	$V_{Cr:VA}^{A,bcc}$	$2.0358 \times 10^{-5} T \exp\left(-\frac{p}{p_{cut'}}\right) + 4.5466 \times 10^{-12} T^3 \exp\left(-\frac{p}{p_{cut}}\right)$
	$V_{Cr:VA}^{C,bcc}$	1.5202×10^{-6}
	$V_{Cr:VA}^{K,bcc}$	$4.9076 \times 10^{-12} + 3.7849 \times 10^{-16} T \exp\left(-\frac{p}{p_{cut}}\right)$
	$V_{Cr:H}^{0,bcc}$	1.2283×10^{-5}

	$V_{Cr:H}^{A,bcc}$	$2.0358 \times 10^{-5} T \exp\left(-\frac{p}{p_{cut}}\right) + 4.5466 \times 10^{-12} T^3 \exp\left(-\frac{p}{p_{cut}}\right)$
	$V_{Cr:H}^{C,bcc}$	1.5202×10^{-6}
	$V_{Cr:H}^{K,bcc}$	$4.9076 \times 10^{-12} + 3.7849 \times 10^{-16} T \exp\left(-\frac{p}{p_{cut}}\right)$
	$G_{Cr:H}^{hcp}$	$G_{Cr}^{SER} + \frac{1}{2} G_{H_2}^{SER} - 1.0368 \times 10^4 + 6.3176 \times 10^1 T$
<i>hcp</i>	$V_{Cr:H}^{0,hcp}$	8.4916×10^{-6}
	$V_{Cr:H}^{A,hcp}$	$2.1048 \times 10^{-5} T \exp\left(-\frac{p}{p_{cut}}\right) + 1.4263 \times 10^{-8} T^2 \exp\left(-\frac{p}{p_{cut}}\right)$
	$V_{Cr:H}^{C,hcp}$	1.7374×10^{-6}
	$V_{Cr:H}^{K,hcp}$	$5.4958 \times 10^{-12} + 1.5275 \times 10^{-18} T^2 \exp\left(-\frac{p}{p_{cut}}\right)$
	$G_{Cr:H}^{fcc}$	$G_{Cr}^{SER} + \frac{1}{2} G_{H_2}^{SER} - 7.6176 \times 10^3 + 6.0127 \times 10^1 T$
	$V_{Cr:H}^{0,fcc}$	8.6038×10^{-6}
<i>fcc</i>	$V_{Cr:H}^{A,fcc}$	$2.7706 \times 10^{-5} T \exp\left(-\frac{p}{p_{cut}}\right) + 6.1163 \times 10^{-9} T^2 \exp\left(-\frac{p}{p_{cut}}\right) + 7.6773 \times 10^{-12} T^3 \exp\left(-\frac{p}{p_{cut}}\right)$
	$V_{Cr:H}^{C,fcc}$	8.4338×10^{-7}
	$V_{Cr:H}^{K,fcc}$	$4.3481 \times 10^{-12} + 1.4166 \times 10^{-16} T \exp\left(-\frac{p}{p_{cut}}\right) + 1.3452 \times 10^{-18} T^2 \exp\left(-\frac{p}{p_{cut}}\right)$

4.3. Cr–H–Zr system.

The pressure-composition isotherms of $bcc\text{-Cr}_x\text{Zr}_{1-x}$ ($0 \leq x \leq 1$) alloy were calculated from the combination of the three binary systems Cr–H, Cr–Zr and H–Zr, **Fig. 23. Left side**. The addition of chromium to the alloy results in an increase of the equilibrium pressure at a constant H/M ratio. Furthermore, when the H/M ratio is very low (less than 0.2), the chromium substitution does not significantly increase the equilibrium pressure until $x \sim 0.8$, **Fig. 23. Right side**. Thus, it

is predicted that the thermodynamic behavior of a bcc - $\text{Cr}_x\text{Zr}_{1-x}$ alloy containing a small atomic portion of chromium is similar to the behavior of pure β -Zr alloy from the point of view of the absorption capacity and equilibrium pressure.

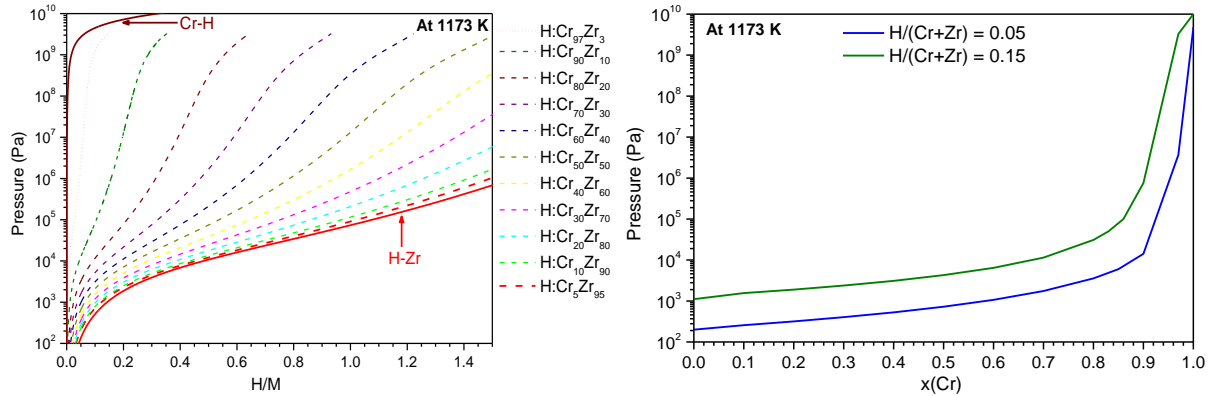


Fig. 23 – **Left side:** Calculated pressure-composition isotherms of extrapolated Cr–H–Zr system at 1173 K. **Right side:** Logarithm of the pressure as a function of the chromium amount at $\text{H}/(\text{Cr}+\text{Zr})= 0.05$ and 0.15 .

One alloy of composition $\text{Cr}_5\text{Zr}_{95}$ was prepared by induction furnace melting of bulk elements under argon. The ingot was turned over and melted six times to ensure homogeneity. It was annealed at 1323 K during 13 days under argon and then quenched to keep the high temperature bcc microstructure. The purity of chromium was 99.99 % and the zirconium was reactor grade. The ingot was cut into pieces before the X-ray and hydriding experiments. Our synthesized alloy $\text{Cr}_5\text{Zr}_{95}$ was fully β -Zr with a cell parameter of 3.5540 Å, **Fig. 24**. The diffuse scattering in the X-ray pattern comes from the sample holder because the sample was a small slice instead of a powder. The hydriding experiments were conducted in a modified Sieverts apparatus under hydrogen (scientific hydrogen 6H_2 from Linde). The measurement was fast enough (3 to 4 hours) to avoid the decomposition of the bcc phase during the hydrogenation.

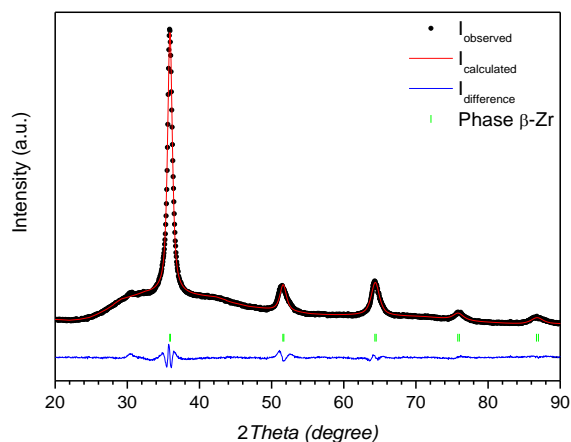


Fig. 24 – X-Ray diffraction profile of $\text{Cr}_5\text{Zr}_{95}$.

The calculated isotherms at 1073 K, 1123 K and 1173 K have been plotted in **Fig. 25** and are compared with the experimental pressure-composition curves. An excellent agreement with the thermodynamic prediction is observed testifying the quality of the thermodynamic description of the three systems and in particular that of the Cr–H system made in the present work.

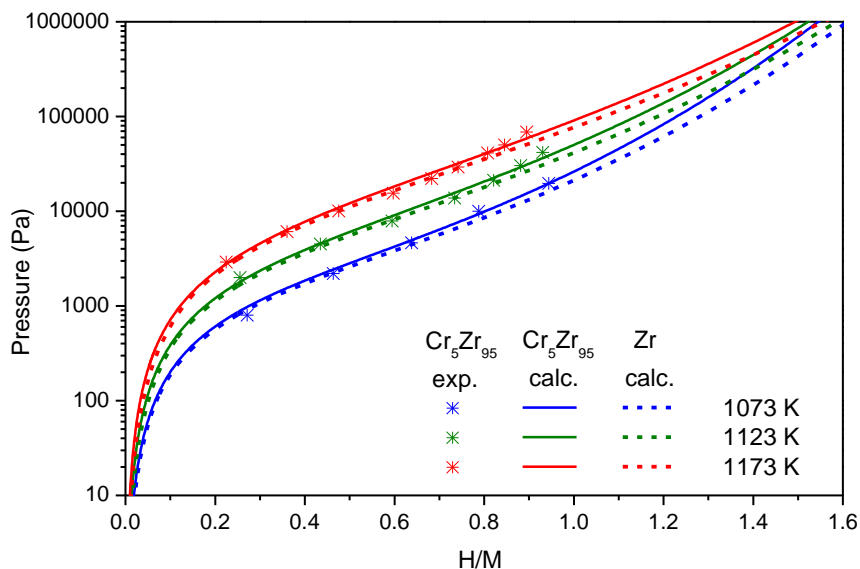


Fig. 25 – Calculated pressure-composition isotherms of extrapolated Cr–H–Zr system at 1073 K, 1123 K and 1173 K and our experimental measurements. Curved for pure Zr are given for comparison.

5. Conclusion

The high-pressure chromium–hydrogen binary system has been assessed for the first time using the Calphad method and the Parrot module of Thermo-Calc. The use of both experimental data from the literature and our DFT and phonon calculations appeared to be essential to depict this system up to few gigapascal. For this purpose, two models, Joubert et al. [13] and Lu et al. [12], have been used to describe the behavior of hydrogen at high pressure and the pressure dependence of condensed phases respectively. The reliability of our models was tested experimentally by comparing our pressure-composition isotherms against our extrapolation of Cr–H–Zr system. As mentioned in the introduction, this Cr–H assessment is a first step and it may be useful as input to develop a multicomponent *bcc* related hydrogen database.

ASSOCIATED CONTENT

Supporting Information

The Supporting Information is available free of charge.

The Thermo-Calc Database Format (TDB) is given. This file is the thermodynamic database on the Cr phases and Cr–H system obtained from this work.

AUTHOR INFORMATION

Corresponding Author

Jean-Marc Joubert – Institut de Chimie et des Matériaux Paris Est, Université Paris Est Creteil, CNRS - UMR 7182, 2 rue Henri Dunant, 94320 Thiais, France; orcid.org/0000-0001-7266-1850 ; Email: jean-marc.joubert@cnrs.fr

Authors

Maxime Dottor – Institut de Chimie et des Matériaux Paris Est, Université Paris Est Creteil, CNRS - UMR 7182, 2 rue Henri Dunant, 94320 Thiais, France

Jean-Claude Crivello – Institut de Chimie et des Matériaux Paris Est, Université Paris Est Creteil, CNRS - UMR 7182, 2 rue Henri Dunant, 94320 Thiais, France; orcid.org/0000-0002-4849-2556

Author Contributions

The manuscript was written through contributions of all authors. All authors have given approval to the final version of the manuscript.

DECLARATION OF INTERESTS

The authors declare that they have no known competing financial interests or personal relationships that could have appeared to influence the work reported in this paper.

ACKNOWLEDGEMENTS

DFT and phonon calculations were performed using HPC resources from GENCI–CINES (Grant A0100906175). M.D. thanks Université Paris Est Creteil for financial support of the PhD research of the first author.

REFERENCES

- [1] Chen Z, Ma Z, Zheng J, Li X, Akiba E, Li H. Perspectives and challenges of hydrogen storage in solid-state hydrides. *Chin J Chem Eng* 2020;S1004954120304729. <https://doi.org/10.1016/j.cjche.2020.08.024>.
- [2] Akiba E, Iba H. Hydrogen absorption by Laves phase related BCC solid solution. *Intermetallics* 1998;6:461–70. [https://doi.org/10.1016/S0966-9795\(97\)00088-5](https://doi.org/10.1016/S0966-9795(97)00088-5).
- [3] Chen P, Zhu M. Recent progress in hydrogen storage. *Mater Today* 2008;11:36–43. [https://doi.org/10.1016/S1369-7021\(08\)70251-7](https://doi.org/10.1016/S1369-7021(08)70251-7).
- [4] Møller KT, Jensen TR, Akiba E, Li H. Hydrogen - A sustainable energy carrier. *Prog Nat Sci Mater Int* 2017;27:34–40. <https://doi.org/10.1016/j.pnsc.2016.12.014>.
- [5] Abe JO, Popoola API, Ajenifuja E, Popoola OM. Hydrogen energy, economy and storage: Review and recommendation. *Int J Hydrog Energy* 2019;44:15072–86. <https://doi.org/10.1016/j.ijhydene.2019.04.068>.
- [6] Hirscher M, Yartys VA, Baricco M, Bellosta von Colbe J, Blanchard D, Bowman RC, et al. Materials for hydrogen-based energy storage – past, recent progress and future outlook. *J Alloys Compd* 2020;827:153548. <https://doi.org/10.1016/j.jallcom.2019.153548>.
- [7] Marques F, Balcerzak M, Winkelmann F, Zepon G, Felderhoff M. Review and outlook on high-entropy alloys for hydrogen storage. *Energy Environ Sci* 2021;14:5191–227. <https://doi.org/10.1039/D1EE01543E>.
- [8] Stein F, Leineweber A. Laves phases: a review of their functional and structural applications and an improved fundamental understanding of stability and properties. *J Mater Sci* 2021;56:5321–427. <https://doi.org/10.1007/s10853-020-05509-2>.
- [9] Baranowski B, Bojarski K. Formation of Chromium Hydride from Metallic Chromium and High-Pressure Gaseous Hydrogen. *Rocz Chem* 1972;46:525–8.
- [10] Fukai Y, Mizutani M. Phase Diagram and Superabundant Vacancy Formation in Cr-H Alloys. *Mater Trans* 2002;43:1079–84. <https://doi.org/10.2320/matertrans.43.1079>.
- [11] Marizy A, Geneste G, Loubeyre P, Guigue B, Garbarino G. Synthesis of bulk chromium hydrides under pressure of up to 120 GPa. *Phys Rev B* 2018;97:184103. <https://doi.org/10.1103/PhysRevB.97.184103>.
- [12] Lu X-G, Selleby M, Sundman B. Implementation of a new model for pressure dependence of condensed phases in Thermo-Calc. *Calphad* 2005;29:49–55. <https://doi.org/10.1016/j.calphad.2005.04.001>.
- [13] Joubert J-M, Crivello J-C, Deffrennes G. Modification of Lu’s (2005) high pressure model for improved high pressure/high temperature extrapolations. Part I: Modeling of platinum at high pressure/high temperature. *Calphad* 2021;74:102304. <https://doi.org/10.1016/j.calphad.2021.102304>.

- [14] Straumanis ME, Weng CC. The precise lattice constant and the expansion coefficient of chromium between +10 and +60 °C. *Acta Crystallogr* 1955;8:367–71. <https://doi.org/10.1107/S0365110X55001254>.
- [15] Vasyutinskii BM, Kartmazov GN, Finkel VA. Problems of the structure of chromium at temperatures of 700–1700 °C. *Fiz Met Metalloved* 1961;12:141–2.
- [16] Bolef DI, de Klerk J. Anomalies in the Elastic Constants and Thermal Expansion of Chromium Single Crystals. *Phys Rev* 1963;129:1063–7. <https://doi.org/10.1103/PhysRev.129.1063>.
- [17] Ross RG, Hume-Rothery W. High temperature X-ray metallography: I. A new debye-scherrer camera for use at very high temperatures II. A new parafocusing camera III. Applications to the study of chromium, hafnium, molybdenum, rhodium, ruthenium and tungsten. *J Common Met* 1963;5:258–70. [https://doi.org/10.1016/0022-5088\(63\)90031-6](https://doi.org/10.1016/0022-5088(63)90031-6).
- [18] Müller S, Dünner Ph. Bestimmung des Gitterparameters von Chromim Temperaturbereich von 20 °C bis 1500 °C. *Z Für Naturforschung* 1965;20a:1225–6.
- [19] Combley FH. An investigation of the crystal structure of antiferromagnetic chromium. *Acta Crystallogr Sect B* 1968;24:142–4. <https://doi.org/10.1107/S0567740868001810>.
- [20] Gordienko VA, Nikolaev VI. Magnetic Anomalies of the Thermal Expansion of Chromium. *JETP Lett* 1971;14:6–9.
- [21] Koumelis CN. The thermal expansion coefficient of chromium in the temperature region of 3 to 80 °C. *Phys Status Solidi A* 1973;19:K65–9. <https://doi.org/10.1002/pssa.2210190157>.
- [22] Makeev VV, Popel PS. Density and coefficients of thermal expansion of nickel, chromium, and scandium in the solid and liquid states. *Teplofiz Vysok Temp* 1990;28:704–7.
- [23] Stankus SV. The density of vanadium and chromium at high temperatures. *Teplofiz Vysok Temp* 1993;31:565–8.
- [24] Dubrovinskaia NA, Dubrovinsky LS, Saxena SK, Sundman B. Thermal expansion of Chromium (Cr) to melting temperature. *Calphad* 1997;21:497–508. [https://doi.org/10.1016/S0364-5916\(98\)00007-8](https://doi.org/10.1016/S0364-5916(98)00007-8).
- [25] Erfling HD. Studien zur thermischen Ausdehnung fester Stoffe in tiefer Temperatur. II. *Ann Phys* 1939;34:136–60. <https://doi.org/10.1002/andp.19394260204>.
- [26] Hidnert P. Thermal expansion of cast and of swaged chromium. *J Res Natl Bur Stand* 1941;27:113–24. <https://doi.org/10.6028/jres.027.003>.
- [27] Fine ME, Greiner ES, Ellis WC. Transitions in Chromium. *J Met* 1951;3:56–8. <https://doi.org/10.1007/BF03398956>.
- [28] White GK, Andrikidis C. Thermal expansion of chromium at high temperature. *Phys Rev B* 1996;53:8145–7. <https://doi.org/10.1103/PhysRevB.53.8145>.
- [29] Ming L, Manghnani MH. Isothermal compression of bcc transition metals to 100 kbar. *J Appl Phys* 1978;49:208–12. <https://doi.org/10.1063/1.324325>.
- [30] Tkacz M. High pressure studies of the FCC chromium hydride. *Rev High Press Sci Technol* 1998;7:1735–41.
- [31] Young DA, Cynn H, Söderlind P, Landa A. Zero-Kelvin Compression Isotherms of the Elements $1 \leq Z \leq 92$ to 100 GPa. *J Phys Chem Ref Data* 2016;45:043101. <https://doi.org/10.1063/1.4963086>.
- [32] Palmer SB, Lee EW. The elastic constants of chromium. *Philos Mag J Theor Exp Appl Phys* 1971;24:311–8. <https://doi.org/10.1080/14786437108227390>.
- [33] Katahara KW, Nimalendran M, Manghnani MH, Fisher ES. Elastic moduli of paramagnetic chromium and Ti-V-Cr alloys. *J Phys F Met Phys* 1979;9:2167–76. <https://doi.org/10.1088/0305-4608/9/11/008>.
- [34] Lahteenkorva EE, Lenkkeri JT. Effects of magnetic order on elastic moduli of chromium. *J Phys F Met Phys* 1981;11:767–73.
- [35] White GK, Roberts RB, Fawcett E. Thermal expansion of Cr and CrV alloys. I. Experiment. *J Phys F Met Phys* 1986;16:449–59. <https://doi.org/10.1088/0305-4608/16/4/009>.
- [36] Mcqueen RG, Marsh SP. Equation of state for nineteen metallic elements from shock-wave measurements to two megabars. *J Appl Phys* 1960;31:1253–69.
- [37] Saito T, Shiraishi Y, Sakuma Y. Density measurement of molten metals by levitation technique at temperature between 1800 and 2200 °C. *Trans Iron Steel Inst Jpn* 1969;71:118–26.
- [38] Errandonea D, Schwager B, Ditz R, Gessmann C, Boehler R, Ross M. Systematics of transition-metal melting. *Phys Rev B - Condens Matter Mater Phys* 2001;63:132104. <https://doi.org/10.1103/PhysRevB.63.132104>.
- [39] Alcock CB, Itkin VP, Horrigan MK. Vapour Pressure Equations for the Metallic Elements: 298–2500K. *Can Metall Q* 1984;23:309–13. <https://doi.org/10.1179/cmqr.1984.23.3.309>.
- [40] Weichselfelder T. Über die Hydride der Metalle Nickel, Kobalt, Eisen und Chrom. *Justus Liebigs Ann Chem* 1926;447:64–77. <https://doi.org/10.1002/jlac.19264470107>.

- [41] Sarry B. Wasserstoffverbindungen von Schwermetallen. II. Zur Darstellung von Schwermetall-Wasserstoff-Verbindungen nach der Methode von SCHLENK und WEICHSELFELDER. *Z Für Anorg Allg Chem* 1955;280:65–77. <https://doi.org/10.1002/zaac.19552800106>.
- [42] Knödler A. Über die Bildung von chromhydrid durch elektrolyse und seine struktur. *Metalloberfläche* 1963;17:161–8.
- [43] Roy RJ, Gibb TRP. The paramagnetic susceptibility of chromium hydride. *J Inorg Nucl Chem* 1967;29:341–5. [https://doi.org/10.1016/0022-1902\(67\)80036-8](https://doi.org/10.1016/0022-1902(67)80036-8).
- [44] Stock AD, Hardcastle KI. Phase and composition analysis of chromium hydride. *J Inorg Nucl Chem* 1970;32:1183–6. [https://doi.org/10.1016/0022-1902\(70\)80113-0](https://doi.org/10.1016/0022-1902(70)80113-0).
- [45] Baranowski B, Bojarski K, Tkacz M. Cr-H and Cr-D Systems in High-Pressure Region. *Rev Phys Chem Jpn* 1975:577–9.
- [46] Miura Y, Yokota S, Fukai Y, Watanabe T. Hydrogen Dissolution and Structural Changes in Electrodeposited Cr Films. *Mater Trans* 2005;46:963–8. <https://doi.org/10.2320/matertrans.46.963>.
- [47] Antonov VE, Beskrovnyy AI, Fedotov VK, Ivanov AS, Khasanov SS, Kolesnikov AI, et al. Crystal structure and lattice dynamics of chromium hydrides. *J Alloys Compd* 2007;430:22–8. <https://doi.org/10.1016/j.jallcom.2006.05.021>.
- [48] Tkacz M, Baranowski B. The equations of state of Pd, Ni, Cr, and their hydrides in high pressure at room temperatures. *Pol J Chem* 1992;66:1301–11.
- [49] Snavely CA. The Theory for the Mechanism of Chromium Plating; A Theory for the Physical Characteristics of Chromium Plate. *Trans Electrochem Soc* 1947;92:537. <https://doi.org/10.1149/1.3071841>.
- [50] Snavely CA, Vaughan DA. Unit cell dimension of face-centered cubic chromium hydride and space groups of two chromium hydrides. *J Am Chem Soc* 1949;71:313–4.
- [51] Pépin CM, Dewaele A, Geneste G, Loubeyre P, Mezouar M. New Iron Hydrides under High Pressure. *Phys Rev Lett* 2014;113:265504. <https://doi.org/10.1103/PhysRevLett.113.265504>.
- [52] Albrecht G, Doenitz F-D. Neutronenbeugung an “hexagonalem Chrom.” *Phys Status Solidi III* 1963;K249–52.
- [53] Peisl H. Lattice strains due to hydrogen in metals. In: Alefeld G, Völkl J, editors. *Hydrog. Met. I*, vol. 28, Berlin, Heidelberg: Springer Berlin Heidelberg; 1978, p. 53–74. https://doi.org/10.1007/3540087052_42.
- [54] Li J, Lu X-G, He Y. Molar Volume of Fcc Phase in the Ni-Cr-Mo System. *Adv Mater Res* 2014;936:1209–15. <https://doi.org/10.4028/www.scientific.net/AMR.936.1209>.
- [55] Smithson H, Marianetti CA, Morgan D, Van der Ven A, Predith A, Ceder G. First-principles study of the stability and electronic structure of metal hydrides. *Phys Rev B* 2002;66:144107. <https://doi.org/10.1103/PhysRevB.66.144107>.
- [56] Miwa K, Fukumoto A. First-principles study on 3 d transition-metal dihydrides. *Phys Rev B* 2002;65:155114. <https://doi.org/10.1103/PhysRevB.65.155114>.
- [57] Martin E. Ein Beitrag zur Frage der Aufnahmefähigkeit des reinen Eisens und einiger seiner Legierungselemente für Wasserstoff und Stickstoff. *Arch Für Eisenhüttenwes* 1929;3:407–16.
- [58] Luckemeyer-Hass L, Schenck H. Löslichkeit von Wasserstoff in einigen Metallen und Legierungen. *Arch Für Eisenhüttenwes* 1932;6:209–14.
- [59] Mazaev AA, Avarbe RG, Vilk YN. Features of solubility of hydrogen in metals of subgroup 6. *Russ J Phys Chem USSR* 1968;42:338–40.
- [60] Arnoult WJ, McLellan RB. Thermodynamics of transition metal-hydrogen solid solutions. *Acta Metall* 1973;21:1397–403. [https://doi.org/10.1016/0001-6160\(73\)90089-8](https://doi.org/10.1016/0001-6160(73)90089-8).
- [61] Shapovalov VI, Serdyuk NP, Dolzhenkov VI. Phase diagram of Cr-H. *Dokl Akad Nauk Ukr SSR Ser A* 1981;3:88–90.
- [62] Sieverts A, Gotta A. Über die Eigenschaften einiger Metallwasserstoffe. *Z Für Anorg Allg Chem* 1928;172:1–31. <https://doi.org/10.1002/zaac.19281720102>.
- [63] Randzio S, Bojarski K. Calorimetric measurements of the heat of hydrogen desorption from nonstoichiometric chromium hydrides. *Rocz Chem* 1974;48:1375–8.
- [64] Wolf G. Specific heat of chromium hydride CrH_x from 11 to 300 °K. *Phys Status Solidi A* 1971;5:627–32. <https://doi.org/10.1002/pssa.2210050312>.
- [65] Weinstein M, Elliott JF. The solubility of hydrogen in liquid pure metals Co, Cr, Cu and Ni. *Trans Metall Soc AIME* 1963;227:285–6.
- [66] Shapovalov VI. Metal-Hydrogen Phase Diagrams in the Vicinity of Melting Temperatures. Proc. 1999 Int. Symp. Liq. Met. Process. Cast. St. Fe N. M. February 21–24, Research Org.: Sandia National Labs., Albuquerque, NM (US); Sandia National Labs., Livermore, CA (US): 1999, p. 330–43.
- [67] Baranowski B, Bojarski K. Free-Energy of Formation of Chromium Hydride. *Rocz Chem* 1972;46:1403–9.

- [68] Poniatovskii EG, Belash IT. Formation and decomposition of chromium hydride at temperatures up to 400°C and hydrogen pressures up to 20 kbars. *Dokl Akad Nauk SSSR* 1976;229:1171–3.
- [69] Baranowski B. The decomposition pressure of chromium hydride at 150°C. *Rocz Chem* 1971;45:499–500.
- [70] Perdew JP, Burke K, Ernzerhof M. Generalized Gradient Approximation Made Simple. *Phys Rev Lett* 1996;77:3865–8.
- [71] Kresse G, Furthmüller J. Efficient iterative schemes for ab initio total-energy calculations using a plane-wave basis set. *Phys Rev B* 1996;54:11169–86.
- [72] Kresse G, Joubert D. From ultrasoft pseudopotentials to the projector augmented-wave method. *Phys Rev B* 1999;59:1758–75.
- [73] Monkhorst HJ, Pack JD. Special points for Brillouin-zone integrations. *Phys Rev B* 1976;13:5188–92. <https://doi.org/10.1103/PhysRevB.13.5188>.
- [74] Parlinski K, Li ZQ, Kawazoe Y. First-Principles Determination of the Soft Mode in Cubic ZrO_2 . *Phys Rev Lett* 1997;78:4063–6. <https://doi.org/10.1103/PhysRevLett.78.4063>.
- [75] Togo A, Tanaka I. First principles phonon calculations in materials science. *Scr Mater* 2015;108:1–5.
- [76] Jansson B. Thesis TRITA–MAC 0234. Division of Physical Metallurgy, Royal Institute of Technology, Stockholm, Sweden, 1984.
- [77] Andersson J-O, Helander T, Höglund L, Shi P, Sundman B. Thermo-Calc & DICTRA, computational tools for materials science. *Calphad* 2002;26:273–312. [https://doi.org/10.1016/S0364-5916\(02\)00037-8](https://doi.org/10.1016/S0364-5916(02)00037-8).
- [78] Zhong Y, Macdonald DD. Thermodynamics of the Zr–H binary system related to nuclear fuel sheathing and pressure tube hydriding. *J Nucl Mater* 2012;423:87–92. <https://doi.org/10.1016/j.jnucmat.2012.01.016>.
- [79] Lafaye P, Toffolon-Masclat C, Crivello J-C, Joubert J-M. Experimental investigations and thermodynamic modelling of the Cr–Nb–Sn–Zr system. *Calphad* 2019;64:43–54. <https://doi.org/10.1016/j.calphad.2018.11.002>.
- [80] SGTE Substance database, version 3. <http://www.crct.polymtl.ca/sgte/index.php?what=1&databases=1&ssub=1> n.d.
- [81] Dinsdale AT. SGTE data for pure elements. *Calphad* 1991;15:317–425.
- [82] Joubert J-M. A Calphad-type equation of state for hydrogen gas and its application to the assessment of Rh–H system. *Int J Hydrog Energy* 2010;35:2104–11. <https://doi.org/10.1016/j.ijhydene.2010.01.006>.
- [83] Hillert M, Staffansson L-I. Regular-solution model for stoichiometric phases and ionic melts. *Acta Chem Scand* 1970;24:3618–3626. <https://doi.org/10.3891/acta.chem.scand.24-3618>.
- [84] Bourgeois N, Crivello J-C, Saengdeejing A, Chen Y, Cenedese P, Joubert J-M. Thermodynamic Modeling of the Ni–H System. *J Phys Chem C* 2015;119:24546–57. <https://doi.org/10.1021/acs.jpcc.5b06393>.
- [85] Zinkevich M, Mattern N, Handstein A, Gutfleisch O. Thermodynamics of Fe–Sm, Fe–H, and H–Sm systems and its application to the hydrogen–disproportionation–desorption–recombination (HDDR) process for the system Fe₁₇Sm₂–H₂. *J Alloys Compd* 2002;339:118–39. [https://doi.org/10.1016/S0925-8388\(01\)01990-9](https://doi.org/10.1016/S0925-8388(01)01990-9).
- [86] Joubert J-M. CALPHAD Modeling of Metal–Hydrogen Systems: A Review. *J Met* 2012;64:1438–47. <https://doi.org/10.1007/s11837-012-0462-6>.
- [87] Hillert M, Jarl M. A model for alloying in ferromagnetic metals. *Calphad* 1978;2:227–38.
- [88] Inden G. The role of magnetism in the calculation of phase diagrams. *Phys B* 1981;103:82–100. [https://doi.org/10.1016/0378-4363\(81\)91004-4](https://doi.org/10.1016/0378-4363(81)91004-4).
- [89] Grover R, Getting IC, Kennedy GC. Simple Compressibility Relation for Solids. *Phys Rev B* 1973;7:567–71. <https://doi.org/10.1103/PhysRevB.7.567>.
- [90] Perdew JP, Ruzsinszky A, Csonka GI, Vydrov OA, Scuseria GE, Constantin LA, et al. Restoring the Density-Gradient Expansion for Exchange in Solids and Surfaces. *Phys Rev Lett* 2008;100:136406. <https://doi.org/10.1103/PhysRevLett.100.136406>.
- [91] Yu S, Jia X, Frapper G, Li D, Oganov AR, Zeng Q, et al. Pressure-driven formation and stabilization of superconductive chromium hydrides. *Sci Rep* 2015;5:17764. <https://doi.org/10.1038/srep17764>.
- [92] Khan HR, Raub ChJ. Properties of chromium hydride. *J Common Met* 1976;49:399–406. [https://doi.org/10.1016/0022-5088\(76\)90051-5](https://doi.org/10.1016/0022-5088(76)90051-5).
- [93] Nowak B, Żoga OJ, Niedźwiedź K, Tkacz M, Żolnierczyk Z. ⁵³Cr knight shift and magnetic susceptibility of hexagonal CrH_{0.93}. *Phys B Condens Matter* 1994;193:102–8. [https://doi.org/10.1016/0921-4526\(94\)90058-2](https://doi.org/10.1016/0921-4526(94)90058-2).
- [94] Antonov VE, Sholin IA. Proving the contact rules for phase regions: Implications to phase diagrams of metal–hydrogen systems. *J Alloys Compd* 2015;645:160–5. <https://doi.org/10.1016/j.jallcom.2015.01.086>.